

# Quantum Chaos = Volume-Law Spatiotemporal Entanglement

Neil Dowling<sup>1,\*</sup> and Kavan Modi<sup>1,2,†</sup>

<sup>1</sup>*School of Physics & Astronomy, Monash University, Victoria 3800, Australia*

<sup>2</sup>*Centre for Quantum Technology, Transport for New South Wales, Sydney, NSW 2000, Australia*

(Dated: October 28, 2022)

Chaotic systems are highly sensitive to a small perturbation, be they biological, chemical, classical, ecological, political, or quantum. Taking this as the underlying principle, we construct an operational notion for quantum chaos. Namely, we demand that the whole future state of a large, isolated quantum system is highly sensitive to past multitime operations on a small subpart of that system. This immediately leads to a direct link between quantum chaos and volume-law spatiotemporal entanglement. Remarkably, our operational criterion already contains the routine notions, as well as the well-known diagnostics for quantum chaos. This includes the Peres-Loschmidt Echo, Dynamical Entropy, and Out-of-Time-Order Correlators. Our principle therefore unifies these existing diagnostics within a single structure. Within this framework, we also go on to quantify how several mechanisms lead to quantum chaos, such as unitary designs. Our work paves the way to systematically study exotic many-body dynamical phenomena like Many-Body Localisation, many-body scars, measurement-induced phase transitions, and Floquet dynamics. We anticipate that our work may lead to a clear link between the Eigenstate Thermalization Hypothesis and quantum chaos.

## I. INTRODUCTION

Chaos as a principle is rather direct; a butterfly flaps its wings, and leads to an effect many times bigger than itself. This effect arises in a vast array of fields, from economics to meteorology.

Quantum chaos, on the other hand, is not well understood and lacks a universally accepted definition. There is a vast web of, often inconsistent, quantum chaos diagnostics in the literature [1, 2], which leads to a muddy picture of what this concept actually means. In contrast, classically chaos is a complete framework. If one perturbs the initial conditions of a chaotic dynamical system, they see an exponential deviation of trajectories in phase space, quantified by a Lyapunov exponent. Trying to naively extend this to quantum Hilbert space immediately falls short of a meaningful notion of chaos, as the unitarity of isolated quantum dynamics leads to a preservation of fidelity with time. How then, can there possibly be non-linear effects resulting from the linearity of Schrödinger's equation? We will see that the structure of entanglement holds the key to this conundrum.

In the 1980s much effort was made to understand quantum chaos primarily as the cause of classical chaos [3–6]: attempting to identify the properties that an underlying quantum system requires in order to exhibit chaos in its semiclassical limit. An example of this was the empirical connection between random matrix theory and the Hamiltonians of classically chaotic systems [3]. Re-

cently, with experimental access to complex many-body quantum systems with no meaningful classical limit, and given progress in related problems such as the black hole information paradox [7, 8] and the quantum foundations of statistical physics [9–11], quantum chaos as a research program has renewed interest across a range of research communities. In this context a complete structure of quantum chaos, independent of any classical limit, is wanting.

In this work we approach quantum chaos from an operational perspective. We first identify the underlying definition of chaos as a starting point, containing all the necessary facets, and build a quantum butterfly effect from this fundamental principle. Chaos as a theory-independent principle is best summarised through the analogy of the butterfly effect: a butterfly flaps its wings, and this local perturbation leads to a macroscopic effect, such as a weather event. Using this analogy as inspiration, chaos can be boiled down to the following statement: *Chaos is a deterministic, highly non-local and strong sensitivity in the future, to a past, local perturbation.*

We construct a genuinely quantum measure for chaos based solely on this statement. We adapt this principle into the theory of quantum processes and exploit their multitime structures. Namely, we use a tool from quantum information theory – process-state duality – to show that this dynamical measure is isomorphic to a static property of a quantum state. This then leads us to an alarmingly simple, but deep, conclusion: quantum chaos is nothing but the structure of spatiotemporal entanglement. Put in other words, if a quantum process can create volume-law entangled states from many different (possibly multitime) area-law inputs – be it processes,

\* neil.dowling@monash.edu

† kavan.modi@monash.edu

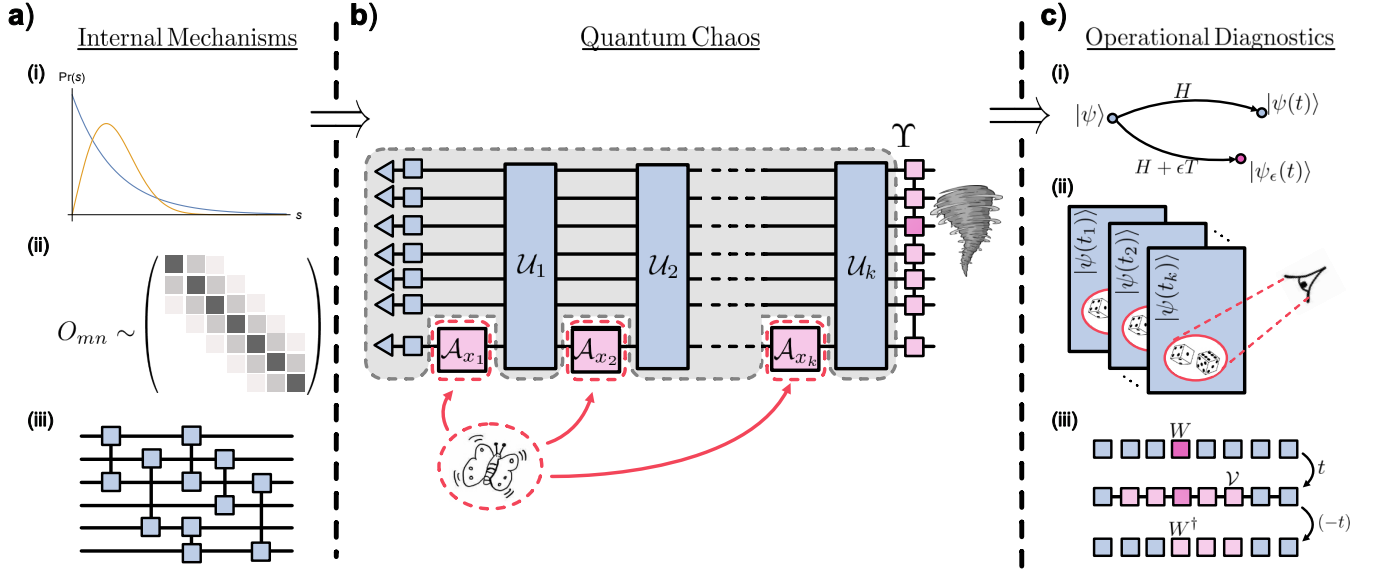


FIG. 1. A schematic of the causes, structure, and effects of quantum chaos. **a)** Internal mechanisms of chaos are the intrinsic properties of the dynamics that lead to chaotic effects. For example, properties of the Hamiltonian such as level spacing statistics (i) and the Eigenstate Thermalisation Hypothesis (ii), or properties of the quantum circuit describing the dynamics such as whether it forms a unitary design (iii). **b)** In this work we will construct the general quantum butterfly effect, and from this argue that chaos reduces to the volume-law spatiotemporal entanglement structure of the process describing the dynamics. This principle forms the stepping stone between causal mechanisms of chaos and operational diagnostics of chaos. **c)** Operational diagnostics for quantum chaos. Some popular probes include (i) The Peres-Loschmidt Echo, also known as fidelity decay or Loschmidt echo, which is the measure of the deviation between states, for evolution under a perturbed compared to an unperturbed Hamiltonian [12, 13]; (ii) The Dynamical Entropy, which quantifies how much information one gains asymptotically from repeatedly measuring a subpart of a quantum system [4, 14–16]; and (iii) Out-of-Time-Order Correlators (OTOCs), which measure the rate at which two locally operators anticommute with time [17–20].

channels, or measurements/preparations – we call that process chaotic. We will consider a number of explicit examples of quantum butterfly protocols that support this result. Further affirming the validity of our approach, our criterion is stronger than and encompasses existing operational diagnostics. We show this explicitly for out-of-time-order correlators (OTOCs), Peres-Loschmidt Echo, and dynamical entropy<sup>[21]</sup>. That is, we can *derive* each of these three popular chaos diagnostics, previously justified only heuristically, starting only from a natural construction of the quantum butterfly effect. However, we will show that these previous diagnostics are all insufficient, whereas we argue that this principle of quantum chaos is both necessary and sufficient. Under the umbrella of the spatiotemporal entanglement structure, this work therefore unifies these apparently inconsistent diagnostics.

Next, we show that there are several known mechanisms for quantum processes that lead to quantum chaos. In particular, we show that both Haar random unitary dynamics and random circuit dynamics – which lead to approximate  $t$ -design states – are highly likely to generate processes which satisfy our operational criterion for quantum chaos. Our results also open the possibility of systematically studying other internal mechanism thought to generate quantum chaos, e.g. Wigner-Dyson statistics [3], or the Eigenstate Thermalisation Hypothe-

sis (ETH) [22–24].

In Fig. 1, we classify previous concepts of quantum chaos in the context of our results; laying out a schematic of the landscape this field. In particular, we identify operational diagnostics as quantities which *may* detect chaos, but fall short of a catch-all classification. These are the observable probes of chaos. On the other hand, internal mechanisms are the properties of a quantum dynamical system which lead to chaotic effects. The centre of this figure represents the main result of this work: identifying the structure of quantum chaos which we show is the primitive behind the observations of the operational diagnostics.

Previous works have hinted at the connection between some of the previous, heuristic diagnostics for quantum chaos [25–27]. These often rely on averages over Haar and/or thermal ensembles. Our approach is different, in that we work solely within a deterministic, pure-state setting, uncovering the structure of chaos without any need to average over operators or dynamics.

We begin in Section II by reviewing the two main tools which we will use to arrive at our results. These are: the process tensor formalism, which is the natural language of quantum stochastic processes; and entangle-

ment structure, the qualitative classes of entanglement which asks how the Schmidt rank scales with subsystem size, and therefore whether exponential information is needed to most efficiently represent a state. Then, in Section III we will construct the quantum butterfly effect from first principles, and arrive at the central, titular result of this work. From there, in Section IV we show how this principle can be used to derive (generalisations of) the three previous chaos diagnostics we introduced above: the Peres-Loschmidt Echo, the Dynamical entropy, and the OTOC. In this context we also analyse paradigmatic examples of regular and chaotic processes. Next, in Section V we explore some analytic examples of the quantum butterfly effect, strengthening the claim that this quantity reduces to volume-law entanglement structure. Finally, in Section VI we show that random dynamics - both fully Haar random and that generated by unitary designs - typically lead to chaos. We finish with concluding remarks where we speculate about the wide range of future applications that this foundational work promotes.

## II. TOOLS: QUANTUM PROCESSES AND THE STRUCTURE OF SPATIOTEMPORAL ENTANGLEMENT

The results of this work rely on the novel application of ideas from quantum tensor network theory, and multitime quantum processes, to the overarching problem of chaos in isolated many-body systems. We here only give an overview of the relevant facets of these topics, and refer the reader to a selection of excellent reviews for a more complete introduction to the process tensor framework [28] and tensor networks [29, 30].

### A. Multitime Quantum Processes

Consider a finite dimensional quantum system. A quantum process is a quantum dynamical system under the effect of multitime interventions on some accessible local space  $\mathcal{H}_S$ . The dynamics can then be dilated to a system-environment  $\mathcal{H}_S \otimes \mathcal{H}_E$ , such that the total isolated  $S + E$  evolves unitarily on this extended space. A  $k$ -step process tensor is the mathematical description of a such a process, encoding all possible spatiotemporal correlations in a single object; analogous to a density matrix for single-time quantum measurement.

Measurement is necessarily invasive in quantum mechanics. Therefore, to construct such a multitime description we need to understand quantum measurements which includes the resultant state. Arbitrary interventions are defined by the action on  $S$  by external *instru-*

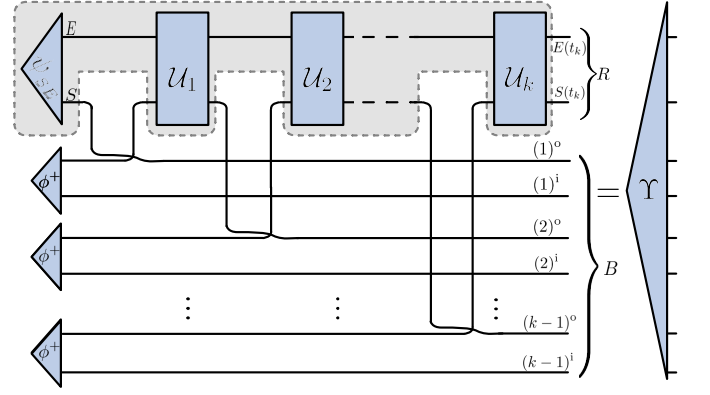


FIG. 2. Tensor network diagram of the construction of the Choi state of a process tensor through the generalized Choi-Jamiolkowski isomorphism [31, 32]. This means that input indices are put on equal footing with output indices, through appending a maximally entangled ancilla system  $|\phi^+\rangle$  at each time, and inserting half of this state into the process. The final output state of this protocol encodes all multitime correlations: a process tensor. A multitime expectation value can then be computed in this representation by finding the Hilbert Schmidt inner product between this (normalised) Choi state and the (supernormalised) Choi state of a multitime instrument, as well as tracing over the environment space  $E(t_k)$ ; as in Eq. (4). The system  $S$  denotes the singletime space where instruments act, and the environment  $E$  the dilated space such that all dynamics are unitary. Here the independent Hilbert spaces are labeled such that  $(\ell)^i$  ( $(\ell)^o$ ) is the input (output) system space  $S$  at time  $t_\ell$ , showing that the final output  $|\Upsilon\rangle$  corresponds to a  $(2k + 1)$ -body density matrix.

ments, which mathematically are trace-non-increasing completely positive (CP) and time independent maps,  $\mathcal{A}$ . If a instrument is also trace-preserving (TP), then it is deterministic; e.g. a unitary map or a complete measurement (POVM). If an instrument is trace-decreasing, then it is non-deterministic; e.g. a particular measurement result. The trace of the outgoing state corresponds to the probability of this outcome occurring out of a complete measurement described by the set  $\mathcal{J} = \{\mathcal{A}_{x_i}\}$ ,

$$\mathbb{P}(x_j|\mathcal{J}) = \text{tr}[\rho'] := \text{tr}[\mathcal{A}_{x_j}(\rho)], \quad (1)$$

Note that in this work, calligraphic font Latin letters will generally be used for such superoperators - that is a map of a (density) operator - while standard font uppercase Latin or lowercase Greek letters will be used for operators (matrices).

Similarly, for multiple, consecutive interactions of a single quantum system at different times, the (in general subnormalised) outgoing state is

$$\rho' = \text{tr}_E[\mathcal{U}_k \mathcal{A}_{x_k} \mathcal{U}_{k-1} \dots \mathcal{U}_1 \mathcal{A}_{x_1}(\rho(t_1))] \quad (2)$$

where  $\mathcal{U}_j(\sigma) := e^{-iH(t_j-t_{j-1})}\sigma e^{iH(t_j-t_{j-1})}$  is the unitary superoperator describing the dilated system-environment (SE) evolution, and the trace is the partial trace over the environment ( $E$ ). For non-deterministic instruments, the trace of this final state gives the probability of measuring a sequence of outcomes  $x_1, x_2, \dots, x_k$ . We can also

write down the full pure state on  $SE$  at the end, without tracing over the environment

$$|\Upsilon_{R|\vec{x}}\rangle := |\psi'_{SE}\rangle = U_k A_{x_k} U_{k-1} \dots U_1 A_{x_1} |\psi_{SE}\rangle, \quad (3)$$

where we have rewritten this as the conditional state of a subpart of process  $\Upsilon$ , and will explain exactly what this means below. As everything is pure here, there is no need to consider superoperators or density matrices, and left multiplication by matrices is a sufficient description. While the first construction is more operationally reasonable – particularly for describing open system dynamics – this pure state process Eq. (3) will be central to defining the structure of quantum chaos in our results. We can write the probability of observing the outcomes  $x_1, x_2, \dots, x_k$  in the process, using the following succinct representation

$$\mathbb{P}(x_k, \dots, x_1 | \mathcal{J}_k, \dots, \mathcal{J}_1) = \text{tr}[\rho'] =: \text{tr}[\Upsilon_B \mathbf{A}_{\vec{x}}^T]. \quad (4)$$

Here we have split the uncontrollable dynamics and the protocol  $\mathbf{A}_{\vec{x}}$  into independent tensors, where  $\Upsilon_B$  is a density matrix. This is related to some pure state  $|\Upsilon\rangle$ , corresponding to collecting the full final  $SE$  state as in Eq. (3), via

$$\Upsilon_B := \text{tr}_R[|\Upsilon\rangle\langle\Upsilon|]. \quad (5)$$

We will define exactly what these mean below. Here, we have gathered the multitime Hilbert space where the instruments act into a single label,

$$\mathcal{H}_B \equiv \mathcal{H}_{S(t_{k-1})}^{\text{io}} \cdots \otimes \mathcal{H}_{S(t_2)}^{\text{io}} \otimes \mathcal{H}_{S(t_0)}^{\text{io}} \quad (6)$$

called the ‘butterfly’ space  $B$ , where  $\mathcal{H}_{S(t_j)}^{\text{io}} \equiv \mathcal{H}_{S(t_j)}^{\text{i}} \otimes \mathcal{H}_{S(t_j)}^{\text{o}}$ .  $\mathcal{H}^{\text{i}}$  represents the input space to the process, while  $\mathcal{H}^{\text{o}}$  represents the output. The ‘remainder’ space  $R$  – the full outgoing system plus environment at the end of the protocol, where the ‘butterfly’ does not act – is

$$\mathcal{H}_R \equiv \mathcal{H}_{S(t_k)}^{\text{o}} \otimes \mathcal{H}_{E(t_k)}^{\text{o}}. \quad (7)$$

All of these are clearly labeled in Fig. 2. It will become apparent in the following section why we name these spaces so.

Eq. (4) can be derived using the generalised Choi–Jamiołkowski Isomorphism (CJI) [31, 33], to split the dynamics and initial state into a single object  $\Upsilon_B$ , independent of the choice of instruments encoded in the tensor  $\mathbf{A}_{\vec{x}}$ . In Fig. 2 we detail the CJI. It essentially corresponds to inputting half of a maximally entangled state ( $|\phi^+\rangle$ ) to the process at each time step, which results in a  $(2k)$ –body unnormalised quantum state  $\Upsilon_B$  which is in one-to-one correspondence to the process itself.  $\Upsilon_B$  is called a process tensor [28, 31, 33] (also called a ‘quantum comb’ [34, 35] or ‘process matrix’ [36, 37]).  $|\Upsilon\rangle$ , on the other hand, is what we call a *pure process tensor*. It corresponds to retaining the full  $SE$  pure state at the end

of the multitime protocol. It can be written succinctly as

$$|\Upsilon\rangle := |\mathbf{U}_k\rangle * \cdots * |\mathbf{U}_1\rangle * |\psi_{SE}(t_1)\rangle, \quad (8)$$

where  $*$  is the Link product, corresponding to composition of maps within the Choi representation [34], and is essentially a matrix product on the  $E$  space, and a tensor product on the  $S$  space. A ket of an operation  $A$  corresponds to the single-time Choi state

$$|A\rangle := (A \otimes \mathbb{1}) |\phi^+\rangle, \quad (9)$$

by the usual single-time CJI – channel-state duality [38].

In Eq. (4), all outside influences are then encoded in the independent Choi state  $\mathbf{A}_{\vec{x}}^T$ , where  $T$  denotes the transpose. This can similarly be constructed using the CJI. For independent instruments at each intervention time, which are also pure instruments – those with a rank-1 Choi state – we have

$$|\vec{x}\rangle = |x_k\rangle \otimes \cdots \otimes |x_1\rangle, \quad (10)$$

where each single-time state is constructed as in Eq. (9). Then the multitime instrument  $\mathbf{A}_{\vec{x}}$  takes the simple form of a convex mix of pure instruments. Given this construction, Eq. (4) is the multitime generalisation of the Born rule [35, 39].

The key point here is that through the CJI we have reduced all possible correlations of a dynamical multitime experiment to a single quantum state,  $|\Upsilon\rangle$ . This means that all the machinery from many-body physics is available to describe multitime effects. A subtle difference from the single-time case is that the normalisation of these Choi states do not exactly correspond to the normalisation of states and projections. Instruments are taken to be supernormalised, while processes have unit normalisation

$$\text{tr}[\Upsilon] = 1, \quad \text{and} \quad \text{tr}[\mathbf{A}_{\vec{x}}] \leq d_S^{2k}, \quad (11)$$

where the inequality is saturated for deterministic instruments, that is if they are CPTP. This ensures that the multitime Born rule (4) gives well defined probabilities. For example, a sequence of unitary maps should give unit probability for any process tensor  $\Upsilon_B$ . This is immediate to check for example for the maximally noisy process which has a uniformly mixed Choi state,

$$\text{tr}[\mathbf{U}_k^T \Upsilon_B^{(\text{H})}] = \frac{1}{d_S^{2k}} \text{tr}[\mathbf{U}_k] \stackrel{!}{=} 1. \quad (12)$$

This process will be relevant later; see the discussion around Eq. (21).

Therefore, dynamical properties of a process such as: non-Markovianity [28, 33, 36, 40, 41], temporal correlation function equilibration [42, 43], stochastic process classicality [44, 45], multipartite entanglement in



time [46], and other many-time properties [47], can all be clearly defined in terms of properties of the quantum state  $|\Upsilon\rangle$ . However, the temporal entanglement structure is largely unexplored, and we will show that this has vast implications for understanding chaotic, complex, and regular quantum dynamics. We will first describe exactly what is meant by entanglement structure in the usual spatial setting of quantum mechanics.

## B. Entanglement structure and Bond dimension

Any pure quantum state  $|\psi\rangle_{AB}$  on  $\mathcal{H}_A \otimes \mathcal{H}_B$  can be decomposed across any bipartition  $A : B$  via the Schmidt decomposition,

$$|\psi\rangle_{AB} = \sum_{i=1}^{\chi} \lambda_i |\alpha_i\rangle_A |\beta_i\rangle_B, \quad (13)$$

where  $\langle \alpha_i | \alpha_j \rangle = \delta_{ij} = \langle \beta_i | \beta_j \rangle$ .  $\chi$  is called the *bond dimension* or *Schmidt rank*, dictating intuitively how much of the subsystems are entangled with each other. The bond dimension is equal to one if and only if the state is separable across  $A : B$ . Using this decomposition, one can iteratively increase the size of the subsystem  $A$ , and determine how the bond dimension scales. If  $\chi$  is bounded by a constant  $D < d_A$  for any  $A$  with dimension up to  $d_A < d_{AB}/2$ , this is called area-law scaling. In this case, a state can be written efficiently as Matrix Product State (MPS) [29, 48, 49]. In this exact representation, instead of needing  $d^n$  complex numbers to describe the full Hilbert space of an  $n$ -body state with local dimension  $d$ , the MPS requires only  $nD^2$ . This is clearly an efficient representation if  $nD^2 < d^n$ . This is always the case with increasing large  $n$  if  $D$  is constant, which defines area-law states. Despite being introduced in order to efficiently simulate the ground state of certain Hamiltonians, it was soon realised that a fundamental property of a state written as an MPS is revealed in the scaling of the bond dimension [50].

We here define a self-contained notion of what volume-law entanglement means, integral to the main result of this work.

**Definition 1.** *A state is said to be volume-law entangled if the minimal information required to exactly represent it scales exponentially with its size. A state is said to be area-law entangled if it can be represented with information of constant size. This is equivalent to the scaling of the Schmidt rank of an MPS representation of the state, with area-law having constant bond dimension  $\chi = D$ , and volume-law having unbounded  $\chi \sim d^n$ .*

Such a property of a quantum state will synonymously be called *entanglement structure*, *entanglement scaling* or *entanglement complexity* throughout this work. We will

see in this work that this property is intrinsically linked to the chaoticity of a quantum process.

In the right three columns of Table I we summarise three distinct entanglement scaling classes. These three classes are qualitatively different, leading to structural difference in the correlations and entanglement within the states. For example, the MPS representation typically models the ground state of local gapped Hamiltonians, while the Multiscale Entanglement Renormalisation Ansatz (MERA) models the ground state of critical Hamiltonians. We will now delve into our main results, interpreting the dynamical meaning behind entanglement structure in the context of quantum processes.

## III. MAIN RESULT: THE QUANTUM BUTTERFLY EFFECT AND SPATIOTEMPORAL ENTANGLEMENT STRUCTURE

The fundamental principle of chaos is that it is a high sensitivity to a perturbation, which is generally taken to be small. We will now argue that quantum chaos naturally falls within this picture. First, we will define completely generally what a perturbation can be, which we call a ‘butterfly’. Then, we will argue that chaos implies that the whole system is highly sensitive to this perturbation, and define precisely what sensitivity means. From this we will construct a genuinely quantum chaos diagnostic, allowing us to determine that the underlying spatiotemporal entanglement structure of a process dictates chaos. We will work within a deterministic setting: an isolated quantum system setting; in terms of pure states and unitary dynamics.

The most general form of a perturbation is a sequence of quantum operations acting on an small and (in-principle) experimentally accessible system  $S$ , see Eq. (1). We further specify these operations to be rank 1, such that we are not injecting any outside stochasticity into a system, given that chaos is deterministic. We call this collection of perturbations a *butterfly*, which is defined precisely below. We define the ‘environment’ space  $E$  as a purification of  $S$  such that the dilated dynamics on space  $SE$  are unitary, just as in Section II A. As described there, the multitime space where this butterfly acts is collected into the Hilbert space label  $B$ , while  $R$  is the remainder – the final system-environment space at the end. This is expressed in Eqs. (6) and (7).

The *quantum butterfly effect* will be built from a comparison between the final conditional (pure) states, after two distinct butterfly protocols labelled by  $\vec{x}$  and  $\vec{y}$

$$\mathcal{D}(|\Upsilon_{R|\vec{x}}\rangle, |\Upsilon_{R|\vec{y}}\rangle). \quad (14)$$

Here,  $\mathcal{D}$  is some metric on pure quantum states, naturally taken to be the fidelity, and the label  $\vec{w} = (w_1, \dots, w_k) \in$

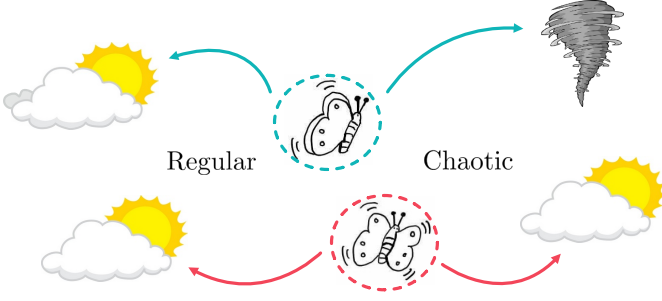


FIG. 3. A cartoon of the butterfly effect. A regular (non-chaotic) system will exhibit an effect proportional to the butterfly's flutter, while a chaotic system will see large, varying, non-local effects from two different butterfly flutters.

$\{\vec{x}, \vec{y}\}$  denotes instruments acting at  $k$  times, such that

$$|\Upsilon_{R|\vec{w}}\rangle := \frac{A_{w_k} U_k \cdots A_{w_2} U_2 A_{w_1} U_1 |\psi_{SE}\rangle}{\sqrt{\langle \psi_{SE} | U_1^\dagger \cdots A_{w_k}^\dagger A_{w_k} \cdots U_1 | \psi_{SE} \rangle}}. \quad (15)$$

This is a normalised state of a bipartite quantum state after a butterfly protocol, which may include a sequence of measurements and preparations on some local system labelled  $S$ , recording the outcomes as  $\vec{w}$ . Alternatively,  $A_{w_i}$  could be a unitary on some subspace, or any other quantum operation which could even be correlated across multiple times. Note that if two butterflies only consist of unitary maps, then the normalisation in the denominator of Eq. (15) is simply equal to one. In the interest of identifying the general form of any quantum butterfly effect, we allow the perturbation to be any pure multitime instrument.

With this we can now explicitly define what we mean by a perturbation which probes chaos.

**Definition 2.** A butterfly is multitime map with some outcome label  $\vec{x}$ , defined by  $k$  rank-1 instruments  $\{A_{x_1}, A_{x_2}, \dots, A_{x_k}\}$ , which takes a  $k$  time pure process  $|\Upsilon\rangle \in \mathcal{H}_B \otimes \mathcal{H}_R$  to a normalised state,

$$|\vec{x}|\Upsilon\rangle = |\Upsilon_{R|\vec{x}}\rangle. \quad (16)$$

Here,  $|\vec{x}\rangle \in \mathcal{H}_B$  is the Choi state of the multitime instrument which defines the butterfly, as in Eq. (10), and the output state  $|\Upsilon_{R|\vec{x}}\rangle$  is defined above in Eq. (15).

Note that butterflies are distinct from the multitime instruments discussed in Section II A only in that we take the normalised output from its action. This is important as we do not wish to consider the probability of a butterfly to occur, only its effect. This is motivated by the principle of chaos as a purely deterministic phenomenon.

We can now map the butterfly effect Eq. (14) to a property of quantum states. Choosing fidelity as the metric, the butterfly effect Eq. (14) can then be written as the

fidelity between the conditional states on subsystem  $R$ , given two distinct projections on subsystem  $B$ ,

$$\begin{aligned} |\langle \Upsilon_{R|\vec{x}} | \Upsilon_{R|\vec{y}} \rangle|^2 &= \frac{|\langle \Upsilon | \vec{x} \rangle \langle \vec{y} | \Upsilon \rangle|^2}{|\langle \Upsilon | \vec{x} \rangle|^2 |\langle \vec{y} | \Upsilon \rangle|^2} \\ &= \frac{|\langle \vec{y} | \Upsilon_B | \vec{x} \rangle|^2}{\langle \vec{x} | \Upsilon_B | \vec{x} \rangle \langle \vec{y} | \Upsilon_B | \vec{y} \rangle}, \end{aligned} \quad (17)$$

where  $\Upsilon_B$  is the reduced state of  $|\Upsilon\rangle$  on  $B$ , as in Eq. (5), and the butterfly Choi states are orthogonal,  $\langle \vec{x} | \vec{y} \rangle = d_B \delta_{\vec{x}, \vec{y}}$ . Given that  $|\Upsilon\rangle$  is a pure state, here we have used its Schmidt decomposition,

$$\begin{aligned} \langle \Upsilon | \vec{x} \rangle \langle \vec{y} | \Upsilon \rangle &= \sum_i \lambda_i \langle \Upsilon_B^{(\alpha_i)} | \langle \Upsilon_R^{(\beta_i)} | (|\vec{x}\rangle_B \langle \vec{y}|_B) \\ &\quad \times \sum_j \lambda_j^* |\Upsilon_B^{(\alpha_j)}\rangle |\Upsilon_R^{(\beta_j)}\rangle \\ &= \sum_i |\lambda_i|^2 \langle \vec{y} | \Upsilon_B^{(\alpha_i)} \rangle \langle \Upsilon_B^{(\alpha_i)} | \vec{x} \rangle \\ &= \langle \vec{y} | \Upsilon_B | \vec{x} \rangle. \end{aligned} \quad (18)$$

Our construction of dynamical quantum chaos then reduces to a static property of a process: given two non-deterministic projections on some small subsystem, how do the leftover states compare? For a chaotic process, butterflies need to have a large effect. This means that orthogonal projections on a large subsystem of the Choi state will (approximately) orthogonalise the remaining state, and so the quantity Eq. (17) will be (approximately) zero. This is the basis of the *quantum butterfly effect*.

To construct the full butterfly effect, there is one further subtlety which we have not yet considered. Consider the cartoon in Fig. 3. In any system, chaotic or otherwise, a 'butterfly flutter' may have an effect proportional to its size, as depicted in the cartoon Fig. 3. Therefore, to define chaos we now demand that the effect of the butterfly protocol is rather large (non-local), as well as strong. More technically, we want to avoid cases where the orthogonalisation resulting from a perturbation resides entirely in a small subspace of  $R$ , yet could be misconstrued as a strong global effect. It is a quirk of the tensor product structure of Hilbert space that distinguishability of a subpart implies distinguishability of the whole. Any orthogonality in the  $R$  space will give a vanishing fidelity in Eq. (17), irrespective of the size of the subspace this orthogonality resides in. We therefore include a notion of *scrambling* as the further specification that the butterfly effect spreads to a large portion of the environment. The expression (17) is currently insufficient to test for this.

We can remedy the quantum butterfly effect, Eq. (17), to include scrambling through the application of a local unitary within the space  $R$ . Consider some few-body unitary  $V$ , which acts on some small subspace  $\bar{R} \subset R$ . We take  $V$  to align the two post-butterfly states on the subspace  $\bar{R}$  upon which it acts. Then if the butterfly has

Class of Dynamics	Temporal Entanglement Structure	Correlation Scaling	Example Circuits
Chaotic	Volume-law: $\chi \sim d^n$	Unbounded	Random Quantum Circuits (brick wall) [51]; $t$ -designs.
Critical/Complex	Sub-volume-law: $\chi \sim \min\{D^{\log(n)}, d^n\}$	$\langle O_n O_{n+\ell} \rangle \sim -\ell$	MERA [52].
Regular	Area-law: $\chi \sim \min\{D, d^n\}$	$\langle O_n O_{n+\ell} \rangle \sim e^{-\ell}$	MPS [49], from staircase circuit [53, 54].

TABLE I. Summary of classification of dynamics in terms of the ability for the unitary process (or circuit describing the process) to create classes of entangled states.  $\chi$  is the bond-dimension, or minimal Schmidt rank across any bipartition of size  $d^n$ ,  $D$  is some constant which is independent of number of ‘sites’  $n$ , and  $\ell$  is some positive integer. The first column describes the qualitative class of dynamics, whereas the next three columns all describe many-body states. Our contribution is the identification of the isomorphism/connection between the first column and the others through the lens of quantum processes and the CJI.

affected the future state on  $R$  strongly, but locally,  $V$  will function to distinguish this as not chaotic. This effect will be elucidated through an example in Section IV D.

Formally, we take the dimension of this ‘aligning’ space  $\bar{R}$  to scale at most polynomially with the size of the butterfly space  $B$ ,

$$\dim(\bar{R}) \sim \text{poly}(d_B) \ll \dim(R). \quad (19)$$

Here we have also made explicit that a butterfly needs to be small to accurately distinguish between chaos and order. A large butterfly may ‘create’ chaoticity, which we discuss in more detail in the discussion Section IV E. Just as the chaos of meteorology means a butterfly flutter may cause a tornado [55], quantum chaos means a quantum butterfly acting on 100 spins may produce a large effect in a system of  $\mathcal{O}(10^{23})$  spins.

We are now in a position to define a complete, genuinely quantum chaos diagnostic  $\zeta(\Upsilon)$ , which we call the quantum butterfly effect. This combines the few-body ‘aligning’ unitary  $V$  together with Eq. (17). For  $|\vec{x}\rangle, |\vec{y}\rangle$  denoting some pair of butterfly Choi states,

$$\begin{aligned} \zeta(\Upsilon) &:= \sup_{\bar{R}, V, \langle \vec{x} | \vec{y} \rangle = 0} (|\langle \Upsilon_{R|\vec{x}} | V | \Upsilon_{R|\vec{y}} \rangle|^2) \\ &= \sup_{\bar{R}, V, \langle \vec{x} | \vec{y} \rangle = 0} \left( \frac{|\langle \vec{y} | \text{tr}_{\bar{R}}(\Upsilon_{B\bar{R}} V) | \vec{x} \rangle|^2}{\langle \vec{x} | \Upsilon_B | \vec{x} \rangle \langle \vec{y} | \Upsilon_B | \vec{y} \rangle} \right). \end{aligned} \quad (20)$$

where  $\text{tr}_{\bar{R}}$  is a partial trace over the subsystem  $\bar{R}$ . The supremum is taken over all subspaces  $\bar{R} \subset R$  up to a dimension satisfying Eq. (19), together with all unitary matrices  $V$  on this space, and then over all projections  $|\vec{x}\rangle$  and  $|\vec{y}\rangle$  which act on the multitime butterfly space  $B$ . While this gives the optimal sensitivity to perturbation of a quantum dynamical system, one may choose any two butterflies in order to probe for chaos, dropping the supremum over  $|\vec{x}\rangle$  and  $|\vec{y}\rangle$  and including dependence over the set of butterflies  $\mathcal{X} := \{|\vec{x}\rangle, |\vec{y}\rangle\}$ . However, for a single choice of perturbation  $\mathcal{X}$ , it may not be possible to determine if the process is chaotic or not, for instance if the butterfly is on a subspace  $B$  which is too small, or

on a very particular subspace. In Section V, we will also consider the average  $\zeta$  over a complete basis of butterflies  $\mathcal{X} = \{|\vec{x}_i\rangle\}_{d_B}$ , in order to capture average chaoticity in a quantum dynamical system. We stress that the normalisation in Eq. (20) is identically equal to one for a butterfly composed of a sequence of unitaries, which is exactly the case for the Peres-Loschmidt Echo. We will show in Section IV A how the Peres-Loschmidt Echo is essentially a weakened version of  $\zeta$ .

If a process is not chaotic, then the fidelity between the two states  $|\Upsilon_{R|\vec{x}}\rangle$  and  $|\Upsilon_{R|\vec{y}}\rangle$  is already (close to) one, and so the supremum over the aligning unitary is (approximately) satisfied trivially for  $V = \mathbb{1}$ . In this case,  $\zeta(\Upsilon, \mathcal{X})$  reduces to the original construction, Eq. (17). Otherwise, the unitary will act to align the part of the state  $\Upsilon_{\bar{R}}$ , and the question of chaos comes down to whether the remaining pure states on  $R \setminus \bar{R}$  are orthogonal. Therefore, the aligning unitary  $V$  makes this quantity a measure of both the strength of the butterfly effect and the spreading of the butterfly effect: the scrambling. These two mechanisms will be investigated further through examples in Section IV.

We summarise the argument of this section thus far with the following definition.

**Definition 3.** *Given the condition on butterfly size given by Eq. (19), we call a quantum process  $|\Upsilon\rangle$  chaotic if  $\zeta(\Upsilon)$ , as defined in Eq. (20), decays with the size of the butterfly,  $d_B$ .*

The quantity  $\zeta(\Upsilon)$  tells us how much is the bulk of the environment the system orthogonalised by a multi-time butterfly ‘flutter’. The scaling of this quantity with the total size of the butterfly  $d_B$  will dictate qualitatively different behaviour, characteristic of chaos or regularity. It will be analysed for some example butterflies and dynamics in Section V. This construction of chaos has so far been motivated through analogy of chaos as a theory-independent principle. We will see in Section IV that it agrees very closely with the Peres-Loschmidt Echo, and is actually a generalisation of it.

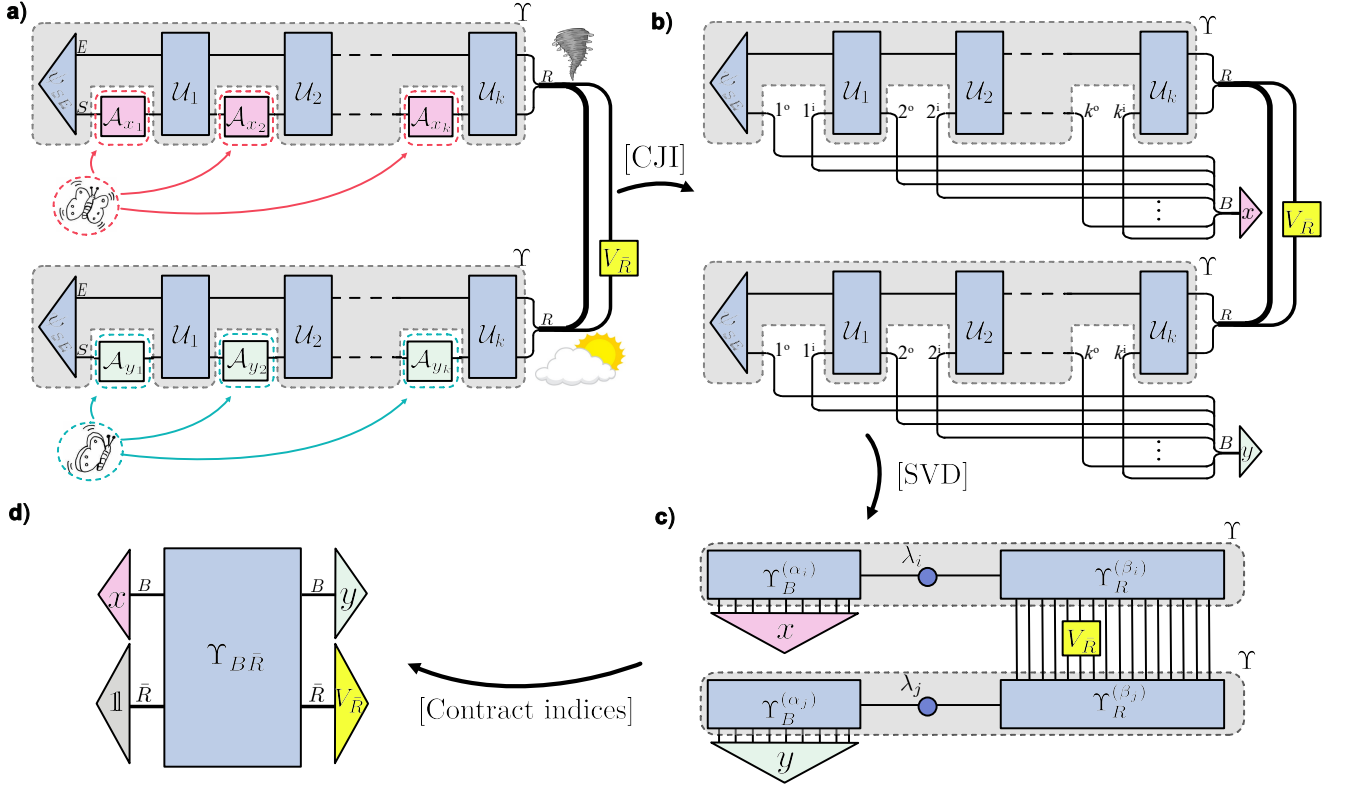


FIG. 4. Three equivalent representations of the quantum butterfly effect; a summary of Section III. **a)** The process representation of a butterfly protocol. Two orthogonal sequences of instruments  $\{\mathcal{A}_{x_i}\}$  and  $\{\mathcal{A}_{y_i}\}$  act at  $k$  times on the system Hilbert space denoted by  $S$ , of a time evolving state  $\psi_{SE}$ . The final pure states on  $SE$  can be compared, with a large distinguishability meaning chaos. Additionally, a unitary  $V$  then aligns some small subpart of the state on  $\bar{R} \subset R$ , which enforces that the butterfly's effect is non-local as well as strong. This is the quantum butterfly effect; Eq. (20) in the text. **b)** Using the CJI, as described in Section II A, the process corresponding to the butterfly protocol can be mapped one-to-one to a quantum state on the spaces  $B$  and  $R$ . Then the quantum butterfly effect corresponds to projecting onto the butterfly space  $B$  with two orthogonal projections  $|\vec{x}\rangle$  and  $|\vec{y}\rangle$ , and comparing the resulting conditional states on  $R$ . These butterfly projections are themselves in one-to-one correspondence to the sequence of instruments in the process representation. **c)** The Schmidt Decomposition (SVD) of  $|\Upsilon\rangle$  allows us to interpret the quantum butterfly effect in terms of the bond between subsystems  $B$  and  $R$ . The cardinality of the set  $\{\lambda_i\}_{i=1}^X$  is the bond dimension (Schmidt rank) which dictates intuitively how much these systems can affect each other in a non-local way. **d)** Contracting the indices, we have reduced the dynamical quantum butterfly effect to the structural properties of the reduced state  $\Upsilon_{B\bar{R}}$ . This representation will be useful primarily in Section V.

Having reduced the most general sense of a quantum chaos diagnostic to the scaling property of a quantum state, we are able to harness the tools of static quantum theory to uncover the essence of quantum chaos. That is, what is the underlying property of a quantum state defined by  $|\Upsilon\rangle$ , which leads to the decay of  $\zeta(\Upsilon)$ ? This consideration leads to the following principle.

**Result 1. (Principle of Quantum Chaos)** *A quantum dynamical process is chaotic if and only if its Choi state has volume-law spatiotemporal entanglement with respect to small, multitime interventions, as defined in Definition 1. It is regular if and only if it has area-law spatiotemporal entanglement with respect to small, multitime interventions. Otherwise we call it complex.*

The need of volume-law is rather intuitive now. Chaos means a butterfly is able to strongly affect a macroscopic

part of the future state. In this case, two different butterfly flutters result in globally different states, as depicted in Fig. 3. The butterfly strongly affecting the final state  $R$  corresponds to large *temporal* entanglement between  $B$  and  $R$ , while this effect being highly non-local means that parts of  $R$  are highly *spatially* entangled with all other parts, up to a resolution of size  $\bar{R}$ . Together this reveals quantum chaos to be the *spatiotemporal* entanglement structure of a process. Then for any process with area-law entanglement, a restricted Schmidt rank directly implies that the butterfly will not be able to affect the state on  $R$  both strongly and non-locally. This is because Eq. (20) will go as the largest singular value of the reduced state  $\Upsilon_B$  with increasing times ( $d_B$ ). There is also a large family of process that have polynomial entanglement. They too will not see a vanishing  $\zeta$  in Eq. (20). As we will see shortly, the Peres-Loschmidt Echo and dynamical entropy both will fail to necessarily detect these



cases, but will necessarily indicate chaos. We outline these three cases in Table I and highlight the fact that, while these scaling laws are well-studied in space, they are not well understood for space-time. This is precisely the innovation that enables us to equate quantum chaos with quantum entanglement in space-time.

Note that the principle of quantum chaos is independent of the instrument, i.e., the butterfly. It is solely a property of the process itself in terms of entanglement scaling. This allows for testing of this principle against any heuristic of quantum chaos to either certify the said heuristic to be chaotic, or otherwise refute it as non-chaotic. It also implies that the manifestation of quantum chaos may be tested for strong or weak butterflies, and many-time or few-time, which turns out to be the distinction between the Peres-Loschmidt Echo and a class of OTOCs.

One might now want to know if chaotic processes exist, based on the principle Result 1. In fact, from concentration of measure results, it is known that most processes generated from Haar random dynamics are exponentially close to the completely noisy process [56],

$$\text{tr}_R[\Upsilon^{(H)}] \approx \frac{1}{d_S^{2k}}, \text{ for } d_B \ll d_R \quad (21)$$

and polynomially close for dynamics sampled from an  $\epsilon$ -approximate  $t$ -design [57]. Clearly such a process has volume-law spatiotemporal entanglement, as it is typically full rank for any  $k$  such that  $d_B = d^{2k} \ll d_E \approx d_R$ . We explore the typicality of chaos in more detail in Section VI.

This single principle of Result 1 offers a simple, complete view of quantum chaos. It dictates the qualitative class of dynamics of a quantum process, possibly detectable using a range of chaos diagnostics. In Section V we will look at some concrete analytic examples to justify that  $\zeta(\Upsilon)$  probes exactly this property of the Choi state  $|\Upsilon\rangle$ . First, we will investigate its relation to previous ideas of quantum chaos.

#### IV. QUANTUM CHAOS DIAGNOSTICS FROM SPATIOTEMPORAL ENTANGLEMENT STRUCTURE

Remarkably, the Principle 1 underlies three of the most popular operational chaos diagnostics which we have described in the introduction. The Peres-Loschmidt Echo reduces to a weakened version of  $\zeta$ ; the dynamical entropy is immediately non-zero for volume-law spatiotemporal entanglement; and OTOC decay will depend on the entanglement scaling of the circuit generating the dynamics. In this section we will show each of these results in turn. However, all of these traditional diagnostics can

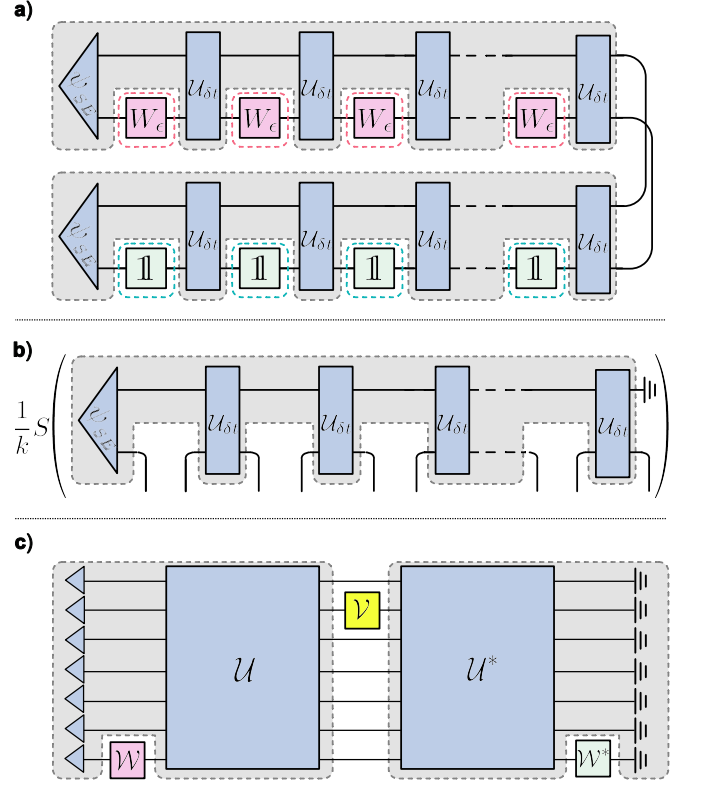


FIG. 5. The quantum process construction for: (a) Peres-Loschmidt Echo, (b) Dynamical entropy, and (c) OTOC. We have colour-coded the OTOC to show its similar structure to the quantum butterfly effect in Fig. III. See Eq. (28) and the surrounding discussion for the precise connection.

misdiagnose a process as non-chaotic. Alternatively, the quantum butterfly effect, quantified by  $\zeta(\Upsilon)$  in Eq. (20), can unambiguously determine whether a quantum process is chaotic or not, albeit given a suitable choice of butterfly space  $B$  and aligning subspace  $\bar{R} \subset E$ .

##### A. Peres-Loschmidt Echo

The Peres-Loschmidt Echo measures the sensitivity of an isolated quantum system to a weak perturbation to the dynamics [12].<sup>[58]</sup> It is equal to the deviation in fidelity between the same initial states evolving unitarily according to some Hamiltonian compared to a perturbed Hamiltonian,

$$|\langle \psi_t | \psi_t^\epsilon \rangle|^2 = |\langle \psi | e^{iHt} e^{-it(H+\epsilon T)} | \psi \rangle|^2. \quad (22)$$

This equivalently measures the distance from the initial state, when a state evolves forward in time, then evolves backwards in time according to imperfect evolution. Exponential decay with time is regarded heuristically to mean quantum chaos. In practice [13, 59], one often needs to discretise the dynamics in order to realise the

perturbation to the Hamiltonian,  $T$ . To do so, one can use the Trotter approximation of the perturbed evolution,

$$\begin{aligned} e^{-it(H+\epsilon T)} &\approx (e^{iH\delta t} e^{i\epsilon T\delta t})^k, \\ &=: (U_{\delta t} W_\epsilon)^k \end{aligned} \quad (23)$$

where  $k\delta t = t$ , which is valid for large  $k$  and small  $\delta t$ . Then, up to Trotter error [60], the Peres-Loschmidt Echo corresponds to the fidelity between two final states, given the application of  $k$  identity channels, compared to  $k$  unitaries which are  $\epsilon$ -close to the identity. From this, we can already see the resemblance between the Peres-Loschmidt Echo and the quantum butterfly effect constructed in the previous section, Eq. (20). The Trotterised Peres-Loschmidt Echo can be seen as a weakened version of  $\zeta$ . For one, no optimisation over an aligning unitary is taken in the Peres-Loschmidt Echo, setting  $V \equiv \mathbb{1}$ . In addition, instead of optimal butterflies, we specify the butterfly set  $\mathcal{X}_{LE}$  to be two chosen projections which are  $(k\epsilon)$ -close. These two projections are respectively the Choi states of a sequence of  $k$  weak unitaries and a sequence of  $k$  identity maps, such that

$$\begin{aligned} |\langle \vec{x} | \vec{y} \rangle| &:= |\langle W_\epsilon^{\otimes k} | \mathbb{1}^{\otimes k} \rangle| \\ &= |\langle W_\epsilon | \mathbb{1} \rangle|^k \\ &= (1 - \epsilon)^k d_S^{2k}. \end{aligned} \quad (24)$$

where we recall that  $d_B = d^{2k}$ . Then for a typical volume-law process, consisting of random dynamics as described around Eq. (21), under the action of any two butterflies of appropriate size we have that  $\Upsilon_B \sim \mathbb{1}/d_B$ , and so typically

$$\begin{aligned} \zeta'(\Upsilon^{(H)}, \mathcal{X}_{LE}) &\approx \frac{|\langle \vec{x} | \mathbb{1}/d_B | \vec{y} \rangle|^2}{\langle \vec{x} | \mathbb{1}/d_B | \vec{x} \rangle \langle \vec{y} | \mathbb{1}/d_B | \vec{y} \rangle} \\ &= (1 - \epsilon)^{2k} d_B^2 (1/d_B^2) \\ &= (1 - \epsilon)^{2k} \\ &\approx e^{-2k\epsilon}, \text{ for small } \epsilon, \\ &\approx 0, \text{ for large } k. \end{aligned} \quad (25)$$

Here we have defined a non-scrambling chaos diagnostic with the prime on  $\zeta$ , indicating that no aligning unitary  $V$  is considered. For an area-law Choi state,  $\zeta'$  will be larger. We will investigate this in more detail in Section IV, where we investigate analytically the ability of  $\zeta'$  to detect entanglement structure.

For a given Trotter error, time evolution corresponds to increasing  $k$ , for a constant  $\delta t$  and  $\epsilon$ . Therefore in Eq. (25) we can see how exponential decay with time stems from the property of entanglement complexity of the Choi state  $|\Upsilon\rangle$ . The choice of temporally local, weak unitaries is key to this exponential time decay with time.

The weakness also allows us to approximate each unitary perturbation to be local, fitting precisely into the

definition of a quantum butterfly effect, Eq. (20). For a weak Hamiltonian perturbation  $T$ , the spectrum of  $T$  is across a small range  $\epsilon$  in comparison to that of  $H$ . This means we can coarse-grain it to only two  $(d_S)$  levels, separated by an energy  $\epsilon$ . In this approximation, the eigenspace of  $T$  is only two  $(d_S)$  dimensional. Labelling it as  $S$ , the weak, global perturbation on  $SE$  is approximately equal to a weak, local perturbation on  $S$ . This argument can similarly be generalised to better approximate the action of  $T$  to be on few-level system, in comparison to the full  $SE$  Hilbert space on which a general  $H$  acts. In this way we can always study the chaos in any single-body quantum systems, e.g. a kicked rotor or top, as a many-body system with a single qubit (qudit) serving as the butterfly space.

We have shown that the Peres-Loschmidt Echo is essentially a weak version of the butterfly effect Eq. (20), with a number of important discrepancies between them. First, the Peres-Loschmidt Echo is composed of two particular butterflies, which need to be unitary, weak, and act on many time steps.  $\zeta$  can be seen as a generalisation of the Peres-Loschmidt Echo from this point of view: optimising over all butterflies which may be arbitrary measurements, channels, etc., and which may act strongly but locally on few or many times. As long as the chosen butterflies do not change the entanglement structure of the process, but only probe it, then it is a valid chaos diagnostic. We discuss some of the subtleties of this in Section IV E. Second, the Peres-Loschmidt Echo has no extra ingredient of an aligning unitary  $V$  acting on the space  $\bar{R} \subset R$ . This distinction means that while the Peres-Loschmidt Echo probes a butterfly having a strong effect, it does not probe the delocalisation of this effect; the scrambling. This will become apparent in Section IV D when we investigate an example of a regular dynamics which is apparently chaotic according to the Peres-Loschmidt Echo. Lastly, the Peres-Loschmidt Echo requires a many-time butterfly, such that exponential decay is achieved in Eq. (24). However, our construction for quantum chaos in Section III is more general in that it does not require a many-time perturbation. This begs the question of what does the butterfly effect look like for a single-time perturbation? We will see that this has the structure of, and is in fact a stronger version of, out-of-time-order correlators.

## B. Out-of-Time-Order Correlators

Consider two local unitary operators  $V_t$  and  $W$  in the Heisenberg picture, with one evolving forward in time unitarily. One can measure how these operators anticommute with time, by investigating the behaviour of the four point out-of-time-order correlator (OTOC) [8, 17–

20],

$$\langle V_t^\dagger W^\dagger V_t W \rangle = 1 - \frac{1}{2} \langle [V_t, W]^\dagger [V_t, W] \rangle. \quad (26)$$

Exponential decay of this correlator is taken to mean the system in question ‘scrambles fast’ and so is chaotic, although this picture is not entirely clear, and has recently been contested [61–65]. While often this expectation value is taken over a thermal state, making the OTOC easier to compute, we here consider pure states as we identify chaos to be an entirely deterministic concept.

Using the process tensor formalism, we can interpret the OTOC and identify the structural properties leading to its decay. This is related to previous work where the OTOC was generalised to an out-of-time-order matrix at three times [66]. Starting with Eq. (26), we can rewrite the OTOC as

$$\begin{aligned} \langle V_t^\dagger W^\dagger V_t W \rangle &= \text{tr}[U_t^\dagger V^\dagger U_t W^\dagger U_t^\dagger V U_t W \rho] \\ &= \text{tr}[W^\dagger U_t^\dagger V U_t W \rho U_t^\dagger V^\dagger U_t] \\ &= \text{tr}[\mathcal{W}^* \mathcal{U}_t^* \mathcal{V} \mathcal{U}_t \mathcal{W}(\rho)], \end{aligned} \quad (27)$$

where  $\mathcal{W}(\sigma) \equiv W(\sigma)W^\dagger$  is a unitary superoperator, and  $\mathcal{U}_t$  is the unitary evolution superoperator forward in time. On the other hand, even though the matrix  $V$  is a unitary *matrix*,  $\mathcal{V}(\sigma) \equiv V(\sigma)\mathbb{1}$  is a linear superoperator which is in general not CP and so not unitary.  $\mathcal{V}^*$  is, however, the inverse map of  $\mathcal{V}$ . This identification is summarised in Fig. IV c). If  $\mathcal{V}$  were a unitary *map* then the OTOC would be equal to  $\text{tr}[\rho]$ , independent of  $V$  and  $W$ .

The OTOC written in this form has a very similar structure to the quantum butterfly effect Eq. (20). If we append a global product state preparation  $\Pi_0$  to the definition of  $\mathcal{W}$  and  $\mathcal{W}^*$ , optimise over  $\mathcal{V}$ , and take  $\mathcal{W}^* \rightarrow \mathcal{W}_\perp$  to be orthogonal to  $\mathcal{W}$  rather than the inverse, we arrive at exactly the quantum butterfly effect for single time butterflies,

$$\begin{aligned} \text{OTOC} &\rightarrow \sup_{\mathcal{V}} \text{tr}[\Pi_0 \mathcal{W}_\perp \mathcal{V}_t \mathcal{W} \Pi_0(\rho)] \\ &= \sup_{\mathcal{V}} |\langle 00 \dots 0 | W U^\dagger V U W | 00 \dots 0 \rangle|^2 \\ &= \sup_{\mathcal{V}} |\langle \Upsilon_{R|W} | V | \Upsilon_{R|W_\perp} \rangle|^2. \end{aligned} \quad (28)$$

In addition, we have taken  $\mathcal{W}$  to be a valid instrument (CP) such that we can consider its left-action on pure states alone,  $\mathcal{W}(\rho) \rightarrow W |\psi\rangle\langle\psi|$  for pure  $\rho = |\psi\rangle\langle\psi|$ . This shows that OTOCs have essentially the structure of a single time quantum butterfly effect protocol Eq. (20). Similarly, a few time butterfly effect has the structure of higher order OTOCs called  $2k$ -OTOCs, investigated in Ref. [26]. The quantum butterfly effect can then be thought of as a stronger version of the (generalised) OTOC. For a fixed aligning unitary  $V$ ,  $\zeta$  is an OTOC.

While Eq. (20) can be seen as a kind of OTOC, it remains to be seen how effective are the class of OTOCs typically examined in the literature, as in Eq. (26). We suspect that when a process is chaotic in accordance with Principle 1, the OTOCs will show a strong decay. However, there may be instances where an OTOC can be spoofed to falsely detect quantum chaos where there is none. For instance, suppose  $\mathcal{W}$  and  $\mathcal{V}$  act within the subspace  $\bar{R}$ , where is a large entanglement, then the OTOC will decay. That is, regular processes with a bond dimension  $D > d_{\bar{R}}$  may be flagged as being chaotic by OTOC, at least for short times.

We have now examined two operation diagnostics, which we shown have the same structure as a few (OTOC) or many-time (Peres-Loschmidt Echo) quantum butterfly effect. We will now investigate an entropic quantity, which probes the entanglement structure of a process given access to only a restricted measurement space.

### C. Dynamical Entropy

The quantum dynamical entropy was originally introduced as the quantum generalisation of the Kolmogorov-Sinai entropy, which quantifies the asymptotic gain of information when a classical system is repeatably measured [4, 14–16]. It quantifies the long-term unpredictability of a dynamics, with positivity indicating chaoticity. Quantum mechanically, measurement necessarily perturbs a system, and comes with its own inherent unpredictability. One can account for the entropy due to a measuring device compared to the process itself [15], but a more elegant solution is to define this quantity in a device independent way [4, 67, 68]. Indeed, classically, Kolmogorov Sinai entropy is the entropy rate of a *stochastic process*, so the natural language of the quantum version of this requires a description of quantum stochastic processes [28, 69]: precisely the process tensor formalism detailed in Section II A.

Formally, dynamical entropy is defined as the asymptotic gain in information when a additional (measurement) steps are added to a quantum process,

$$S_{\text{Dy}}(\Upsilon) := \lim_{k \rightarrow \infty} \frac{1}{k} S(\Upsilon_{B_k}), \quad (29)$$

where  $\Upsilon_{B_k} = \text{tr}_R[\Upsilon]$  is a marginal process on  $k$  time steps, meaning a process with a given dynamics, measured every  $\delta t$  seconds. We do not need to specify what measurement, as the process tensor encodes any possible measurement protocol, fulfilling exactly the role of a spatiotemporal density matrix. See Section II A for details. For such an asymptotic quantity to be non-zero, this strictly requires an infinite dimensional environment. Poincare recurrence would render any finite isolated sys-

tem to have finite total entropy. As we consider unitary dynamics on an isolated, finite dimensional quantum system, we will not take the asymptotic limit precisely. Instead, we define the  $k^{\text{th}}$  dynamical entropy

$$S_{\text{Dy}}^{(k)}(\Upsilon) := \frac{1}{k} S(\Upsilon_{B_k}), \quad (30)$$

where  $k$  is taken to be large, but small enough such that  $d_B = d_S^{2k} \ll d_E \approx d_R$ . From this definition and the principle of chaos as volume-law entanglement, we can directly see that a non-zero  $S_{\text{Dy}}^{(k)}$  serves as a probe for chaos.

**Theorem 2.** *If its dynamical entropy is zero, then a process is not chaotic.*

*Proof.* For a given bond dimension  $\chi$  of a process  $|\Upsilon\rangle$ , the entropy of a reduced state is upper bounded by that of a uniform eigenvalue distribution,

$$S(\Upsilon_B) \leq - \sum_{i=1}^{\chi} \frac{1}{\chi} \log\left(\frac{1}{\chi}\right) = \log(\chi). \quad (31)$$

By Result 1, a process is chaotic if and only if it is volume-law entangled. In this case for any large  $k$  its reduced Choi state  $\Upsilon_{B_k}^{(\text{vol})}$  is full rank. Then  $S(\Upsilon)$  is essentially unbounded, growing linearly to give

$$S_{\text{Dy}}(\Upsilon_B^{(\text{vol})}) \leq \lim_{k \rightarrow \infty} \frac{\log(d_S^{2k})}{k} = 2 \log(d_S) \quad (32)$$

Otherwise, for area-law and sub-volume-law respectively

$$S(\Upsilon_B^{(\text{area})}) \leq \lim_{k \rightarrow \infty} \frac{\log(D)}{k} = 0, \text{ and} \quad (33)$$

$$S(\Upsilon_B^{(\text{sub-vol})}) \leq \lim_{k \rightarrow \infty} \frac{\log(d_S^{\log(k)})}{k} = 0, \quad (34)$$

where the second limit is computed via L'Hôpital's rule.  $\square$

This also approximately holds true if instead the  $k$ -dynamical entropy is considered. What is important is that the dynamical entropy generally exhibits distinct behaviour for area- versus volume-law temporally entangled processes. This simple result shows how closely the construction of dynamical entropy agrees with the principle of quantum chaos derived in this work, despite arriving at it from a starkly different viewpoint - that of the quantum butterfly effect.

For example, the  $k$ -dynamical entropy of a typical process, Eq. (21), is immediately non-zero,

$$\begin{aligned} S_{\text{Dy}}^{(k)}(\Upsilon^{(\text{H})}) &= \frac{S(\frac{1}{d_S^{2k}})}{k} \\ &= \frac{\log(d_S^{2k})}{k} = 2 \log(d_S). \end{aligned} \quad (35)$$

A more precise typicality bound is given in Theorem 2.

It is important to note that the dynamical entropy has not yet been sufficiently justified as an operational quantum chaos diagnostic; merely heuristically as a generalisation of a classical concept. Here we can essentially *derive* dynamical entropy, starting from our principle of Result 1, and connecting it intimately to the Peres-Loschmidt Echo and OTOCs.

One might be tempted to conflate Result 1 - chaos as volume-law entanglement complexity - with non-zero dynamical entropy. The subtle difference is that dynamical entropy measures the *amount* of entanglement entropy across the single bipartition  $B : R$ , whereas chaos is the *structure* of entanglement of the full state of the process  $|\Upsilon\rangle$  on  $BR$ . The principle of quantum chaos is a strictly stronger condition. One could have high entanglement only in the very particular splitting of  $B : R$ , but be described quite simply as an area-law state in a different splitting. We will see in the next section an example of a non-chaotic process that has exactly this structure.

#### D. Example: The Lindblad-Bernoulli Shift

We now consider a somewhat pathological example which is not chaotic, yet looks so for many of the usual diagnostics. First proposed by Lindblad [4] as a quantum counterpart to the Bernoulli shift classical stochastic process, the *Lindblad-Bernoulli shift* describes a discrete dynamics which cyclically permutes an  $n$ -body  $SE$  state, together with some local unitary  $L$  on the  $S$  state,

$$\mathcal{U}(\phi_1 \otimes \phi_2 \otimes \cdots \otimes \phi_n) = (L\phi_2 L^\dagger) \otimes \cdots \otimes \phi_n \otimes \phi_1. \quad (36)$$

We take the total system size  $n$  to be large, compared to the number of time steps  $k$  which we will consider, such that information is essentially lost to the environment. Additionally, we take the total initial  $SE$  state to be in a product state,  $|\psi\rangle_{SE} = \phi_1 \otimes \cdots \otimes \phi_n$ .

Intuitively this system is highly regular. It simply cycles through different states in a straightforward manner, without any scrambling of local information. Any information put in to the process on the system level will never return from the large environment  $E$ . Indeed, in agreement with our principle of quantum chaos Result 1, the Choi state is a product state, which we will now show.

For a single time step, the reduced map  $\Lambda$  is uncorrelated with any other time step, where

$$\Lambda(\rho) := \text{tr}_E(\mathcal{U}_i(|\psi_{SE}\rangle\langle\psi_{SE}|)). \quad (37)$$

Then by the CJI, this channel acting on one-half of a maximally entangled state gives its Choi representation

$$\Lambda_i \otimes \mathbb{1}(|\phi^+\rangle\langle\phi^+|) = L\phi_i L^\dagger \otimes \frac{\mathbb{1}}{d_S}, \quad (38)$$



Then the total process Choi state, for  $k < n$  time steps, is

$$\Upsilon^{(\text{LB})} = \bigotimes_{i=1}^k \left( L\phi_i L^\dagger \otimes \frac{\mathbb{1}}{d_S} \right). \quad (39)$$

Looking at the Peres-Loschmidt Echo for this example,

$$\begin{aligned} \zeta'(\Upsilon^{(\text{LB})}, \mathcal{X}_{\text{LE}}) &= |\langle W_\epsilon^{\otimes k} | \Upsilon^{(\text{LB})} | \mathbb{1}^{\otimes k} \rangle|^2 \\ &= \left| \prod_i^k \langle W_\epsilon | L\phi_i L^\dagger \otimes \frac{\mathbb{1}}{d_S} | \mathbb{1} \rangle \right|^2 \\ &= \left| \prod_i^k \langle \phi^+ | (W_\epsilon^\dagger \otimes \mathbb{1}) (L\phi_i L^\dagger \otimes \frac{\mathbb{1}}{d_S}) | \phi^+ \rangle \right|^2 \\ &= \left| \prod_i^k \text{tr}[L^\dagger W_\epsilon^\dagger L \phi_i] \right|^2 \\ &\leq \left| \prod_i^k \text{tr}[L^\dagger W_\epsilon^\dagger L] \text{tr}[\phi_i] \right|^2 \\ &= |\text{tr}[W_\epsilon]|^{2k} = (1 - \epsilon)^{2k} d_B \approx 0. \end{aligned} \quad (40)$$

where  $|\phi^+\rangle$  is the unnormalised,  $d_S^2$  dimensional maximally entangled state on the space  $\mathcal{H}_S^O \otimes \mathcal{H}_S^I$ , which is equal to the vectorised identity matrix. In the final line we have used that for positive operators,  $\text{tr}(XY) \leq \text{tr}(X)\text{tr}(Y)$ , that  $\phi_i$  is a density matrix, and the weakness of the unitary perturbation  $|\langle W_\epsilon | \mathbb{1} \rangle| = \text{tr}[W_\epsilon] = (1 - \epsilon)d_S$ . Recall that the prime on  $\zeta$  means we neglect any aligning unitary  $V$  on  $\bar{R} \subset R$ . From the smallness of Eq. (40), we see that  $\zeta'$  for the Peres-Loschmidt Echo misclassifies this example as chaotic. It detects that the butterfly orthogonalises the entire final state on  $R$ , but not that this effect scrambles throughout  $R$ .

Adding an aligning unitary  $V$  of size bigger than  $d_B = d_S^{2k}$ , the full quantum butterfly effect given by  $\zeta$  in Eq. (20) will correctly detect the Lindblad-Bernoulli shift as a regular dynamics. This is because  $V$  will act to align the part of the environment where the perturbation effect resides. For simplicity, we consider a  $\zeta'(\Upsilon, \mathcal{X}_{\text{sep}})$  where the butterflies  $\mathcal{X}_{\text{sep}}$  correspond to complete measurements and independent preparations at each time step, inputting pure orthogonal states  $\psi_i^x$  or  $\psi_i^y$  at time  $t_i$ . An analogous computation to Eq. (40), similarly reveals the apparent chaoticity of the Lindblad-Bernoulli shift according to  $\zeta'(\Upsilon, \mathcal{X})$ . However, if we include an optimised aligning unitary  $V$ , from Eq. (20) we arrive at

$$\begin{aligned} \zeta(\Upsilon^{(\text{LB})}, \mathcal{X}_{\text{sep}}) &= \sup_V \left( |\langle \Upsilon_{R|\bar{x}}^{(\text{LB})} | V | \Upsilon_{R|\bar{y}}^{(\text{LB})} \rangle|^2 \right) \\ &= \sup_V \left( |\langle \psi'_{SE|\bar{x}} | V | \psi'_{SE|\bar{y}} \rangle|^2 \right) \\ &= d_B \sup_V |\langle \psi_1^x \dots \psi_k^x \phi_{k+1} \dots \phi_n | V | \psi_1^y \dots \psi_k^y \phi_{k+1} \dots \phi_n \rangle|^2 \\ &= d_B, \end{aligned} \quad (41)$$

where in the final line we have used that  $d_{\bar{R}} \geq d_B = d_S^{2k}$ , with the supremum acting to align the  $k$  orthogonal bodies of the final state, rendering them equal. This large value is indicative of the regularity of the dynamical system. This example illustrates the advantage of the complete quantum chaos diagnostic defined in Eq. (20). If the butterfly's effect spreads, and does not stay on a space of size of order  $d_B$ ,  $V$  would not be able to completely align the final states. This is what scrambling distinguishes.

Much like the Peres-Loschmidt Echo, dynamical entropy cannot tell that the Lindblad-Bernoulli shift is regular. From the Choi representation, Eq. (39), we arrive immediately at a non-zero value,

$$S_{\text{Dy}}^{(k)}(\Upsilon^{(\text{LB})}) = \frac{kS(V\phi_i \otimes \frac{\mathbb{1}}{d_S})}{k} = \log(d_S). \quad (42)$$

In fact, Lindblad originally introduced this as a simple example of a chaotic process, given that it is unpredictable under repeated measurements [4]. The principle of quantum chaos Result 1 shows directly that he was mistaken; that it is highly regular.

The OTOC, however, can detect that this example dynamics is non-scrambling and therefore not chaotic. The Lindblad Bernoulli shift gives an entirely non-decaying OTOC, for any unitary  $V$  and  $W$  on almost any sites. Take  $\mathcal{V}$  to act on site  $j$ , and  $\mathcal{W}$  to act on site  $i$ . Then for a discrete evolution of  $k$  steps,

$$\begin{aligned} \text{OTOC}_{\text{LB}} &= \text{tr}[\mathcal{W}^* \mathcal{U}_k^* \mathcal{V} \mathcal{U}_k (\phi_1 \otimes \dots \otimes \mathcal{W}(\phi_i) \otimes \dots \otimes \phi_n)] \\ &= \text{tr}[\mathcal{W}^* \mathcal{U}_k^* \mathcal{V} (L\phi_{k+1} L^\dagger \otimes \dots \otimes \mathcal{W}(\phi_i) \otimes \dots \otimes \phi_k)] \\ &= \text{tr}[\mathcal{W}^* \mathcal{U}_k^* (L\phi_{k+1} L^\dagger \otimes \dots \otimes \mathcal{W}(\phi_i) \otimes \dots \otimes \mathcal{V}(\phi_{j+k}) \otimes \dots \otimes \phi_k)] \\ &= \text{tr}[\mathcal{W}^* (\phi_1 \otimes \dots \otimes \mathcal{W}(\phi_i) \otimes \dots \otimes \mathcal{V}(\phi_{j+k}) \otimes \dots \otimes \phi_n)] \\ &= \text{tr}[\phi_1 \otimes \dots \otimes (\phi_i) \otimes \dots \otimes \mathcal{V}(\phi_j) \otimes \dots \otimes \phi_n] = 1 \end{aligned} \quad (43)$$

where this is valid as long as  $i \neq j + k$ . Hence if the OTOC for this dynamics is computed as a function of time, i.e. as a function of 'shifts'  $k$ , it will be a delta function which is equal to one for all  $k$  except the time  $k = j - i$ , where it will equal the value  $\text{tr}[\mathcal{W}^* \mathcal{V} \mathcal{W}(\phi_i)]$ . This is certainly not the exponential decay of the OTOC which is characteristic of chaos. Therefore, interestingly OTOCs can detect the regularity of this pathological example. This is consistent with the common interpretation that OTOCs detect scrambling of quantum information. However, as discussed in Section IV B there are also examples of dynamics which suggest it may be insufficient as a chaos diagnostic [61–63].

We note that in Ref. [70] a similar example can be found to the Lindblad-Bernoulli shift, with dynamics generated by Chebotarev-Gregoratti (CG) Hamiltonians. These models would exhibit similar properties of apparent chaoticity according to the Peres-Loschmidt Echo, but for an infinite environment and valid for continuous time evolution. We have examined the simpler Lindblad-Bernoulli Shift here as it is comparably instructive, and

to remain within the paradigm of finite-dimensional isolated quantum systems.

### E. Chaos in Many-body Phenomena

Throughout this section, we have shown how three of the most common quantum chaos diagnostics can be reduced to the scaling of the spatiotemporal entanglement structure of a process. The beauty of this realisation is not only that it unifies quantum chaos into a single, well-defined principle, but also that it allows us to approach existing results and phenomena from a new, simple perspective.

For example, in Ref. [13] it is shown that the Peres-Loschmidt Echo will only detect regularity for a chaotic system - more specifically for a Hamiltonian with a corresponding classically chaotic limit - for very specific Hamiltonian perturbations  $T$ . These perturbations need to exhibit the symmetries of the Hamiltonian under investigation  $H$ , in order for the Peres-Loschmidt Echo to *not* decay exponentially. The claim is then that any system will look chaotic according to Peres-Loschmidt Echo, unless a particularly fine-tuned perturbation is chosen. In our picture, this problem is resolved immediately by the supremum over orthogonal butterflies in the full quantum butterfly effect,  $\zeta$  in Eq. (20).

The physical setup for the quantum butterfly effect - and hence also the Trotterised Peres-Loschmidt Echo - are reminiscent of Floquet systems [71]. A Floquet Hamiltonian is a periodic time-dependent Hamiltonian, such as introducing a periodic kick to an otherwise time independent Hamiltonian. If, in the above construction, we replace the butterflies with strong, global unitaries, they no longer function as a *small* perturbation to the process. Instead, they may change the qualitative behaviour of process, possibly creating chaos or order. For example, the quantum rotor is clearly a regular system, whereas the quantum kicked rotor is chaotic for strong enough kicks [72]. The key difference here, is that a system-wide strong unitary is not a butterfly per se, as it is neither weak nor localised. A strong, global ‘perturbation’ like this can of course change the entanglement structure of the process. Likewise, a strong global butterfly acting on an already chaotic dynamics will likely remain chaotic. However, this is not always the case. If a butterfly acts strongly and locally on the whole system-environment, it can break the volume-law spread of entanglement. This may render a process area-law (or sub-volume-law) and hence regular - as seen in Many-Body Localisation [73, 74], and measurement-induced phase transitions [75, 76]. While these two phenomena were previously surprising, our Principle of Quantum Chaos 1 clearly reveals the mechanism behind this. This shows how our construction allows one to systematically ap-

proach somewhat confounding phenomena in the theory of many-body physics, such as the integrability resulting from Many-Body Localisation, in an entirely straightforward way. Such topics would be interesting to investigate in more detail in future work.

### V. DETECTING CHAOS

To recap, so far in Section III we have built up the quantum butterfly effect, Eq. (20), from reasonable considerations about chaos being fundamentally a sensitivity to perturbation. From this, in Section IV we argued that this reduces to the titular primitive of ‘quantum chaos = volume-law entanglement complexity’, Result 1. We then showed how this underlies three of the most well-accepted quantum chaos diagnostics in the literature.

Now we will take a step back and ask: why does volume-law entanglement equal chaos? And is this equivalent to the reduced state on the butterfly space  $B$  being full-rank,  $\text{rank}(\Upsilon_B) = d_B$ ? We have seen hints that volume-law is necessary and sufficient in the previous section. For example, dynamical entropy measures the amount of entanglement entropy, but is not sufficient for chaos. This example is only full rank for a very particular splitting. The aligning unitary  $V$  in Eq. (20), together with the supremum over it and the space it acts on,  $\bar{R}$ , are key to understanding why entanglement structure is the veracious property underlying quantum chaos. We will choose some examples of butterflies in this section, and see that most butterflies can detect chaos.

We can reinterpret the quantum butterfly effect to further uncover this connection. From Eq. (20),

$$\begin{aligned}\zeta(\Upsilon) &= \sup_{\bar{R}, V, \langle \tilde{x} | \tilde{y} \rangle = 0} \left( |\langle \Upsilon_{R|\tilde{x}} | V | \Upsilon_{R|\tilde{y}} \rangle|^2 \right) \\ &= \sup_{\bar{R}, V, \langle \tilde{x} | \tilde{y} \rangle = 0} \left( |\langle \Upsilon_{(R|\bar{R})|(V \otimes \tilde{x})} | \Upsilon_{(R|\bar{R})|(1 \otimes \tilde{y})} \rangle|^2 \right) \\ &= \sup_{\bar{R}, V, \langle \tilde{x} | \tilde{y} \rangle = 0} \left( \frac{|\langle \tilde{y} | \Upsilon_{B\bar{R}} | \tilde{x} \rangle|^2}{\langle \tilde{x} | \Upsilon_B | \tilde{x} \rangle \langle \tilde{y} | \Upsilon_B | \tilde{y} \rangle} \right),\end{aligned}\quad (44)$$

where

$$\begin{aligned}\langle \tilde{x} | &:= \langle \tilde{x} |_B \langle V |_{\bar{R}}, \text{ and} \\ \langle \tilde{y} | &:= \langle \tilde{x} |_B \langle 1 |_{\bar{R}}.\end{aligned}\quad (45)$$

Here we have identified that the aligning unitary  $V$  on  $\bar{R}$  is essentially equivalent to a larger butterfly, albeit with the appended space  $\bar{R}$  being optimised over; see Fig. III d).

Further, we will choose a particular orthonormal basis of butterflies, which include  $V$ , on the extended space  $B\bar{R}$

$$\mathcal{X}_{B\bar{R}} = \{ |\tilde{x}_i\rangle \}_{i=1}^{d_{B\bar{R}}}. \quad (46)$$

This basis could be composed of unitary instruments, which we will choose later; see Appendix A. We can then define a modified  $\zeta(\Upsilon)$  which more obviously exhibits the fact that the quantum butterfly effect probes the entanglement structure of the process  $\Upsilon$ ,

$$\tilde{\zeta}(\Upsilon, \mathcal{X}_{B\bar{R}}) = \frac{1}{d_{B\bar{R}}^2 - d_{B\bar{R}}} \sum_{i \neq j}^{d_{B\bar{R}}^2 - d_{B\bar{R}}} |\langle \tilde{x}_i | \Upsilon_{B\bar{R}} | \tilde{x}_j \rangle|^2, \quad (47)$$

where we have taken the average butterfly effect over the set  $\mathcal{X}_{B\bar{R}}$ . We will show that evaluating this expression for different butterflies probes the entanglement structure of  $\Upsilon$ .

Including  $V$  as part of the butterfly means that we are determining if the process  $\Upsilon$  is volume-law with respect to the butterfly space together with some part of the remainder space  $\bar{R} \subset R$ . This is because the volume-law property of a state implies that the reduced state for essentially *any* subsystem  $A$ , up to a certain size, will be full rank,

$$\text{rank}(\Upsilon_A^{\text{vol}}) = d_A. \quad (48)$$

For us this will mean that for a butterfly space  $B$  together with any extra part of the remaining space,  $\bar{R} \subset R$ , will be full rank for a volume-law and hence chaotic process. Throughout this section we will probe this through quantities such as the purity - which is bounded by the bond dimension.

### A. Random Butterflies

We will see that most randomly chosen butterflies can distinguish between area-law and volume-law entanglement in states. We will do this by choosing random, orthonormal butterflies on  $B\bar{R}$ , and determining the quantum butterfly effect (47) for these. We additionally take these butterflies to be unitary, such that the denominator is identically equal to one in Eq. (44). We give an explicit construction of this in Appendix A.

In the following,  $\mathbb{P}_{a \sim \mu}$  and  $\mathbb{E}_{a \sim \mu}$  will mean, respectively, the probability and expectation value of the sampling of a random variable  $a$  over the ensemble  $\mu$ , and  $\mu = \text{H}$  is the Haar measure - the unique, unitarily invariant measure on Hilbert space. More details on randomness in Hilbert space will come in Section VI.

We are now in a position to determine exact bounds on the probability of detecting chaos, using such random butterflies.

**Theorem 3. (Random Butterflies are Likely to Detect Chaos)** *For a Haar random choice of orthonormal butterflies  $\mathcal{X}$  across the combined space  $B\bar{R}$  for any choice of space  $\bar{R}$  - or, equivalently, random up to a*

*2-design -  $\tilde{\zeta}(\Upsilon, \mathcal{X})$  from Eq. (47) is highly likely to distinguish between the area-law and volume-law property of  $\Upsilon$ . In particular:*

**A.** *For two unitary, random butterflies  $\mathcal{X} = \{|\tilde{x}\rangle, |\tilde{y}\rangle\}$ , and for  $\delta > 0$ ,*

$$\mathbb{P}_{\mathcal{X} \sim \text{H}} \left\{ \tilde{\zeta}(\Upsilon, \mathcal{X}) \geq \delta \right\} \leq \frac{d_{B\bar{R}}^2 (\text{tr}[\Upsilon_{B\bar{R}}^2] - 1/(d_{B\bar{R}}))}{\delta(d_{B\bar{R}}^2 - 1)} \approx \frac{\text{tr}[\Upsilon_{B\bar{R}}^2] - 1/(d_{B\bar{R}})}{\delta}. \quad (49)$$

**B.** *For a (supernormalised) basis of unitary, random butterflies  $\mathcal{X}_b := \{|\tilde{x}_i\rangle\}_{i=1}^{d_{B\bar{R}}}$ , and  $\text{tr}[\Upsilon_{B\bar{R}}^2] > 2/d_{B\bar{R}}$ , the average  $\tilde{\zeta}$  satisfies*

$$\mathbb{P}_{\mathcal{X} \sim \text{H}} \left\{ \tilde{\zeta}(\Upsilon, \mathcal{X}_b) \geq \frac{\text{tr}[\Upsilon_{B\bar{R}}^2] d_{B\bar{R}}^2}{2(d_{B\bar{R}}^2 - 1)} \right\} \geq \frac{d_{B\bar{R}} (\text{tr}[\Upsilon_{B\bar{R}}^2] - \frac{2}{d_{B\bar{R}}})}{d_{B\bar{R}} + 1} \approx 1 - \frac{2}{\text{tr}[\Upsilon_{B\bar{R}}^2] d_{B\bar{R}}}. \quad (50)$$

*A construction for such a basis is given in Appendix A.*

*Both inequalities are slightly approximated for large  $d_{B\bar{R}}^2$ , such that  $d_{B\bar{R}}^2 \pm 1 \approx d_{B\bar{R}}^2$ .*

This is proven in Appendix B.

The key point is that for volume-law entanglement of the process  $\Upsilon$ , the purity of the reduced state on  $B\bar{R}$  is inversely proportional to the size of the subsystem,

$$\text{tr}[\Upsilon_{B\bar{R}}^2] \sim \mathcal{O}\left(\frac{1}{d_{B\bar{R}}}\right). \quad (51)$$

For a Choi state which is truly volume-law - rather than just maximally entangled across some specific splitting - this is the case for *any* choice of  $\bar{R}$ . So for volume-law, the right hand side of Eq. (49) is close to zero for almost any small  $\delta > 0$ . Therefore, for most random unitary butterflies,  $\tilde{\zeta}$  in Eq. (47) will likely be small for volume-law processes. On the other hand, for area-law process Choi states the purity will not scale with subsystem size, as the rank is bounded by some constant  $D$ . Part B of the theorem certifies this. Eq. (50) says that for a small bond dimension  $D$ , but a relatively large butterfly dimension  $\dim(\mathcal{H}_{B\bar{R}}) \gg d_{B\bar{R}} \gg D$ , almost certainly  $\tilde{\zeta}$  is relatively large compared to the inverse of the butterfly size  $1/d_{B\bar{R}}$ .

This result therefore supports Result 1; that the quantum butterfly effect Eq. (20) probes the entanglement structure of processes.

## B. Schmidt basis

We will now construct a basis of butterflies which exhibits a kind of maximal difference between area- and volume-law entanglement. Recall the Schmidt decomposition, in which basis the reduced state is diagonal,

$$\Upsilon_{BR} = \sum_i^\chi \lambda_i |\alpha_i\rangle \langle \alpha_i|. \quad (52)$$

We will consider two cases: a restricted, constant Schmidt rank  $\chi = D \leq d_{BR}/2$  for area-law, or a full Schmidt rank which scales with the size of the butterfly,  $\chi = d_{BR}$ . We will choose a basis of butterflies  $\mathcal{X}_{\text{sch}}$  composed of the  $d_{BR}$  vectors

$$|\tilde{x}_i^\sigma\rangle := \frac{\sqrt{d_{BR}}}{\sqrt{2}} (|\alpha_i\rangle + \sigma |\alpha_{\bar{i}}\rangle), \quad (53)$$

where  $\sigma = \pm 1$ , and  $|\alpha_i\rangle$  are basis elements in the space complementary to the Schmidt subspace for  $D \leq d/2$  (so  $0 \leq i \leq D$ ), and conversely they are simply  $d_{BR}/2$  Schmidt vectors for  $\chi = d_{BR}$  (so  $0 \leq i \leq d/2$ ). This is an orthogonal basis in both cases,  $\langle \tilde{x}_i^\sigma | \tilde{x}_j^\omega \rangle = \delta_{ij} \delta_{\sigma\omega} d_{BR}$ . Informally, this is somewhat analogous to a generalisation of the plus-minus basis for a qubit.<sup>[77]</sup>

Our bounds on  $\tilde{\zeta}$  will also involve the Quantum Fisher Information (QFI) which, for a particular observable  $A$  and state with Schmidt decomposition  $\rho = \sum_i^\chi \lambda_i |\alpha_i\rangle \langle \alpha_i|$ , is defined as

$$\text{QFI}(\rho, A) := 2 \sum_{i,j}^d \frac{|\lambda_i - \lambda_j|^2}{|\lambda_i + \lambda_j|} \langle \alpha_i | A | \alpha_j \rangle. \quad (54)$$

**Theorem 4.** *Using the butterfly defined by the set  $\mathcal{X}_{\text{sch}}$ , for an area-law state with constant bond dimension  $D \leq d/2$ , and a volume-law state with unbounded bond dimension*

$$\begin{aligned} \tilde{\zeta}(\Upsilon^{(\text{ar})}, \mathcal{X}_{\text{sch}}) &= \frac{2D}{d_{BR}^2 - d_{BR}}, \text{ and} \\ \text{QFI}(\Upsilon^{(\text{vol})}, X) &\leq \tilde{\zeta}(\Upsilon^{(\text{vol})}, \mathcal{X}_{\text{sch}}) \leq \frac{\Delta^2}{4(d_{BR} - 1)\lambda_{\min}^2}, \end{aligned} \quad (55)$$

where we have defined the maximum spectral gap  $\Delta := \max_{i \neq j} |\lambda_i - \lambda_j|$ , the minimum Schmidt coefficient  $\lambda_{\min}$ , which is non-zero as  $\Upsilon^{(\text{vol})}$  is taken to be volume-law and therefore full-rank, and also the Hermitian observable

$$X := \frac{1}{2(d_{BR}^2 - d_{BR})} \sum_{n=1}^{d_{BR}/2} (|\alpha_n\rangle \langle \alpha_n| + |\alpha_{\bar{n}}\rangle \langle \alpha_{\bar{n}}|). \quad (56)$$

A proof of this is supplied in Appendix C.

It is not immediately obvious that this butterfly distinguishes between area- and volume-law spatiotemporal entanglement. However, typical processes are chaotic, as will be investigated in Section VI. As such, reduced states  $\Upsilon_{RB}$  are generally maximum rank and highly concentrated around the maximally mixed state. In this case the maximum spectral gap  $\Delta$  will likely be very small, when compared to  $1/d_{BR}$ . To make sense of this, we can draw analogy with quantum states. Taking  $|\Upsilon\rangle$  to be a quantum state, the following result defines precisely how small  $\Delta$  will be in the typical case.

**Lemma 5.** *For a Haar random state  $|\psi_{BR}\rangle$ , with  $\lambda_{\min}$  and  $\lambda_{\max}$  the minimum and maximum non-zero eigenvalues of  $\Upsilon_B = \text{tr}_R(|\psi_{BR}\rangle \langle \psi_{BR}|)$  respectively, then for  $0 < \delta < 1$*

$$\mathbb{P}\left\{\Delta > \frac{2\delta}{d_B}\right\} \leq 2 \left(\frac{10d_B}{\delta}\right)^{2d_B} \exp\left(-d_E \frac{\delta^2}{14 \ln 2}\right) \quad (57)$$

*Proof.* For economy of notation, we define the right hand side of Eq. (57) as

$$X := 2 \left(\frac{10d_B}{\delta}\right)^{2d_B} \exp\left(-d_E \frac{\delta^2}{14 \ln 2}\right). \quad (58)$$

Then the proof is a simple extension of Lemma III.4 in Ref. [78] (originally from Appendix A in Ref. [79]), which states that

$$\mathbb{P}\left\{\lambda_{\max} > \frac{1}{d_B} + \frac{\delta}{d_B}\right\} \leq \frac{X}{2}, \text{ and} \quad (59)$$

$$\mathbb{P}\left\{\lambda_{\min} < \frac{1}{d_B} - \frac{\delta}{d_B}\right\} \leq \frac{X}{2}. \quad (60)$$

Then, as

$$\begin{aligned} \mathbb{P}\{a + b > A + B\} &\leq \mathbb{P}\{(a > A) \cup (b > B)\} \\ &\leq \mathbb{P}\{a < A\} + \mathbb{P}\{b > B\} \end{aligned} \quad (61)$$

we arrive at our result

$$\begin{aligned} \mathbb{P}\left\{\Delta > \frac{2\delta}{d_A}\right\} &\leq \mathbb{P}\left\{\lambda_{\max} > \frac{1}{d_A} + \frac{\delta}{d_A}\right\} \\ &\quad + \mathbb{P}\left\{-\lambda_{\min} > -\frac{1}{d_A} + \frac{\delta}{d_A}\right\} \\ &\leq X. \end{aligned} \quad (62)$$

□

Now, from this we can see that  $\Delta$  is exponentially small in  $1/d_B$ . As such, typically the upper bound of the butterfly effect for chaotic (volume-law) processes  $\Upsilon^{(\text{vol})}$  according to the set of butterflies  $\mathcal{X}_{\text{sch}}$  is small, in comparison to the upper bound for  $\Upsilon^{(\text{ar})}$ . Therefore, in this case the butterfly set  $\mathcal{X}_{\text{sch}}$  can detect the difference between order and chaos. We expect this typical behaviour



to translate to general, large, volume-law quantum processes. Regarding the lower bound in Eq. (55), the QFI can be related to genuine multipartite entanglement in a many-body system [80]. It would be interesting to investigate this quantity in more detail in the context of quantum chaos as presented in Result 1.

### C. Time Scales of Chaos

We have seen in this section that the quantum butterfly effect measures the entanglement structure of a quantum process, affirming Result 1. There are other considerations about  $\zeta$  which we have not yet considered. One important such notion is the time scales, and the necessity of multi-time butterflies. Quantum chaos is often formulated in terms of time scales, with a rate of deviation or decay, in analogy with the classical case. In the previous section we saw that many time butterflies have the structure of the Peres-Loschmidt Echo, while one (few) time butterflies have the structure of a ( $2k$ -generalised) OTOC. Then how large does the number of times  $k$  need to be to detect chaos? And is there a trade-off between an intermediate number of times  $k$  and many times?

For one, chaos should be defined relative to some time scale. Returning to the butterfly analogy, in relatively short time scales, a butterfly's flutter cannot cause a tornado. This is why the weather can be predicted relatively accurately a few days in advance, but beyond that it becomes far more difficult [55]. Similarly, the quantum butterfly effect Eq. (20) and by extension the principle of quantum chaos are relative to the total time of the process: the time difference between the first butterfly intervention to the final state which is compared,  $t_k - t_0$ .

We can define a butterfly space  $B$  in Eq. (20) either for many or few times,

$$\begin{aligned}\mathcal{H}_B &\equiv \mathcal{H}_{S(t_{k-1})}^{\text{io}} \cdots \otimes \mathcal{H}_{S(t_2)}^{\text{io}} \otimes \mathcal{H}_{S(t_0)}^{\text{io}}, \text{ and} \\ \mathcal{H}_{B'} &\equiv \mathcal{H}_{S'(t_0)}^{\text{io}},\end{aligned}\quad (63)$$

for some large  $k$ . If  $\dim(\mathcal{H}_B) = \dim(\mathcal{H}_{B'})$ , then the definition of  $\zeta$  is essentially the same in both cases. However, the nature of the entanglement complexity that it probes is starkly different.

In the many-time case, a natural scaling with time emerges by progressively considering a butterfly on more and more times. If considering weak instruments, we have seen that one can get exponential decay with time for a chaotic system, as is the case with the Peres-Loschmidt Echo. Similarly, one obtains a scaling with number of measurements in the dynamical entropy, probing exactly the entanglement scaling between the many-time butterfly space  $B$  and the final, total state.

In the few time case, temporal scaling is not appar-

ent. For a single instrument acting as a butterfly, we can bound the butterfly effect Eq. (20) from below by setting  $V \rightarrow \mathbb{1}$ ,

$$\begin{aligned}\zeta(\Upsilon, \mathcal{X}_{t_0}) &\geq |\langle \Upsilon_{R|\vec{x}} | \Upsilon_{R|\vec{y}} \rangle|^2 \\ &= |\langle \psi_{SE|x}(t_1) | \psi_{SE|y}(t_1) \rangle|^2 \\ &= |\langle \psi_{SE|x}(t_0) | U_{t_1}^\dagger U_{t_1} | \psi_{SE|y}(t_0) \rangle|^2 \\ &= |\langle \psi_{SE}(t_0) | x \rangle \langle y | \psi_{SE}(t_0) \rangle|^2\end{aligned}\quad (64)$$

where  $U_{t_1} = \exp(-it_1 H)$ . This bound shows that a single-time butterfly only probes sensitivity in the initial state; its spatial entanglement structure. According to Eq. (64), if the initial state is 'not chaotic', i.e. an area-law state, then neither is the single-time butterfly process. This is similar to comparing the distance between different initial states under unitary evolution, which as we argued in the opening paragraph of the introduction is invariant under unitary dynamics. On the other hand, if the bound (64) is small, then the butterfly has strongly affected the system, albeit in a static sense. By this we mean that the initial state  $|\psi_{SE}(t_0)\rangle$  must be strongly entangled with the environment. In this case the aligning unitary  $V$  needs to be considered, and so the unitary time evolution will not cancel in the fidelity.

We therefore propose that many-time butterflies primarily probe the dynamical chaos of a process, whereas few-time butterflies probe more the static chaos, i.e. the entanglement structure of the initial state. However, these are both integral facets of chaos. Chaos as a principle is both in terms of a dynamics together with an initial state, and so the process tensor framework is the natural language encompassing precisely both of these aspects of a quantum system.

## VI. MECHANISMS FOR GENERATING CHAOS

So far in Section III we have constructed a quantum butterfly effect and identified the structure of quantum chaos, in Section IV we have shown how this connects to existing operational diagnostics, and in Section V we have shown how different explicit butterflies exhibit the entanglement structure of chaos. Looking at the summary of this work, Fig. I, we have yet to discuss the mechanisms of chaos; the underlying properties of the dynamics that lead to chaotic phenomena in a quantum system.

We will now analyse two mechanisms of quantum chaos, and show through these that randomness typically leads to chaos. Consider dynamics which is globally entirely random. More formally, we independently sample unitary matrices from the Haar probability measure  $U_i \sim \mathbb{H}$  between each intervention time in the butterfly protocol. This is the unique, unitarily invariant mea-

sure, meaning that if any ensemble  $\{U_i\}$  is distributed according to the Haar measure, then so is  $\{WU_i\}$  and  $\{U_iW\}$  for any unitary  $W$ . Considering such random unitaries allows one to derive strong concentration of measure bounds. One such famous example for quantum states says that small subsystems of large random pure states are exponentially likely to be maximally mixed [9]. Similarly, processes sampled from Haar random evolution between inventions are highly likely to look like the completely noisy process, for a large environment [56, 57]; see Appendix D. By a completely noisy process, we mean that any measurements result in equal weights, corresponding to the identity matrix Choi state as in Eq. (21).

However, strictly Haar random evolution is not entirely physical, with the full, exponentially large Hilbert space not practically accessible; a ‘convenient illusion’ [81]. On the other hand, quantum circuits with finite depth are far more physical. Further, one can simulate randomness up to the first  $t$  moments using unitary design circuits. An  $\epsilon$ -approximate  $t$ -design can formally be defined such that

$$\mathcal{D}\left(\mathbb{E}_{\mu_{t\epsilon}}\left\{(U^\dagger)^{\otimes s}(X)U^{\otimes s}\right\}-\mathbb{E}_H\left\{(U^\dagger)^{\otimes s}(X)U^{\otimes s}\right\}\right)\leq\epsilon,$$

for all  $s \leq t$ , some appropriate metric  $\mathcal{D}$ , and any observable  $X \in \mathcal{H}^{\otimes s}$ . In words, the  $s$ -fold channel of a  $t$ -design needs to approximately agree with perfectly Haar random sampling. Such design circuits therefore simulate full unitary randomness, but are much more akin to real physical models. For example, an  $\epsilon$ -approximate 2-design can be generated efficiently from two-qubit gates only in polynomial time [82]. This is equivalent to a model of two-body interactions occurring randomly in a system [57].

Just as in Section V, we will consider an orthonormal basis of butterflies on  $B\bar{R}$ ,

$$\mathcal{X}_b = \{|\tilde{x}_i\rangle\}_{i=1}^{d_{B\bar{R}}}, \quad (65)$$

satisfying the normalisation of instruments,  $\langle \tilde{x}_i | \tilde{x}_j \rangle = \delta_{ij} d_{B\bar{R}}$ . From this we will determine the average value of  $\tilde{\zeta}$  across the elements of  $\mathcal{X}_b$ ,

$$\tilde{\zeta}(\Upsilon, \mathcal{X}_b) = \frac{1}{d_{B\bar{R}}^2 - d_{B\bar{R}}} \sum_{i \neq j} \sup_{\tilde{R}} \left( |\langle \tilde{y} | \Upsilon_{B\bar{R}} | \tilde{x} \rangle|^2 \right). \quad (66)$$

We will now give concentration of measure bounds for such unitary designs, together with full Haar random evolution. We will see that sampling from these random dynamics is highly likely to produce a chaotic process.

**Theorem 6. (Most Processes are Chaotic)** Consider a process  $\Upsilon_{B\bar{R}}$  generated by random dynamics, either entirely Haar random denoted by  $H$  or according to an  $\epsilon$ -approximate  $t$ -design denoted by  $\mu_{t\epsilon}$ . Then for a basis of projections  $\mathcal{X}_b$  in which  $\Upsilon_{B\bar{R}}$  is full rank, for any  $\delta > 0$  and for any  $0 < m < t/4$ ,  $\tilde{\zeta}(\Upsilon, \mathcal{X}_b)$  as defined in

Eq. (47) satisfies

$$\mathbb{P}_{U_i \sim \mu} \left\{ \tilde{\zeta}(\Upsilon, \mathcal{X}_b) \geq \frac{\mathcal{J}_\mu(\delta)}{(d_{B\bar{R}} - 1)(1 - \sqrt{\mathcal{J}_\mu(\delta)})^2} \right\} \leq \mathcal{G}_\mu(\delta). \quad (67)$$

Where for a process generated from independent Haar-random evolution,

$$\begin{aligned} \mathcal{J}_H(\delta) &= d_{B\bar{R}}(\mathcal{B} + \delta) \approx d_{B\bar{R}}\left(\frac{1}{d_R} + \delta\right), \text{ and} \\ \mathcal{G}_H(\delta) &= \exp[-C\delta^2] \approx \exp\left[-\frac{(k+1)d_R}{8d_B}\delta^2\right], \end{aligned} \quad (68)$$

while for that generated from an  $\epsilon$ -approximate unitary  $t$ -design

$$\begin{aligned} \mathcal{J}_{\mu_{t\epsilon}}(\delta) &= d_{B\bar{R}}\delta, \text{ and} \\ \mathcal{G}_{\mu_{t\epsilon}}(\delta) &= \frac{\mathcal{F}(d_B, d_R, m, t, \epsilon)}{\delta^m} \end{aligned} \quad (69)$$

The exact definition of  $\mathcal{B}$ ,  $\mathcal{C}$ , and  $\mathcal{F}$  are provided in Eqs. (D2), (D8) and (D10) respectively. The approximations in Eq. (68) are valid for the usual butterfly condition that  $d_R \gg d_B \gg 1$ .

The proof of this theorem is somewhat technical, and has been relegated to Appendix D III. These concentration of measure bounds say that random dynamics is likely to lead to chaos, according to a small butterfly. In particular, for Haar random dynamics, Eq. (68) indicates an exponentially small probability that a given sampling is chaotic. The bounds given here is for the independently sampled evolution between butterfly times, but we note that techniques in Ref. [56] can be used to prove similar bound for repeated dynamics, i.e. a single sample of a unitary evolution matrix that describes all dynamics.

Similarly, random circuits yield a related bound in terms of how well they approximate a unitary design. In this case, Eq. (69) is a polynomially small bound, and in practice can be optimised over the parameter  $m$ . The key point is that both of these probability bounds are small for  $d_E \gg d_{B\bar{R}}$ , which is exactly the butterfly condition of Eq. (19).

While these concentration of measure bounds are for the quantum butterfly effect  $\tilde{\zeta}$ , similar bounds can also be proven for other operational diagnostics considered in Section IV. We will now prove one such bound for the dynamical entropy of a random process.

**Theorem 7.** If a process is generated by random global dynamics between interventions, in the sense described in Theorem 6, then

$$\mathbb{P}_{U_i \sim \mu} \left\{ 2 \ln(d_S) - S_{\text{Dy}}^{(k)}(\Upsilon) \geq \frac{d_S^{2k}}{k \ln(2)} \mathcal{J}_\mu(\delta) \right\} \leq \mathcal{G}_\mu(\delta), \quad (70)$$

where  $\mathcal{J}_\mu(\delta)$  and  $\mathcal{G}_\mu(\delta)$  are defined in Eqs. (68) and (69), but with  $d_{B\bar{R}} \rightarrow d_B$  as no aligning space  $\bar{R}$  is considered for the dynamical entropy.

*Proof.* By the reverse Pinsker inequality,<sup>[83]</sup> we have that

$$\begin{aligned} \ln(d_S^{2k}) - S(\Upsilon_B) &= S(\Upsilon \| \frac{\mathbb{1}}{d_S^{2k}}) \\ &\leq \frac{d_S^{2k}}{\ln(2)} \|\Upsilon_B - \frac{\mathbb{1}}{d_S^{2k}}\|_1^2 \\ &\leq \frac{d_S^{4k}}{\ln(2)} \|\Upsilon_B - \frac{\mathbb{1}}{d_S^{2k}}\|_2^2, \end{aligned} \quad (71)$$

where in the final line we have used that  $\|X\|_1 \leq \sqrt{d}\|X\|_2$ . Using this, we have that

$$\begin{aligned} \mathbb{P}\left\{2\ln(d_S) - S_{\text{Dy}}^{(k)}(\Upsilon) \geq \frac{d_S^{2k}}{k\ln(2)} \mathcal{J}_\mu(\delta)\right\} \\ = \mathbb{P}\left\{\ln(d_S^{2k}) - S(\Upsilon_B) > \frac{d_S^{2k}}{\ln(2)} \mathcal{J}_\mu(\delta)\right\} \\ \leq \mathbb{P}\left\{\frac{d_S^{4k}}{\ln(2)} \|\Upsilon_B - \frac{\mathbb{1}}{d_S^{2k}}\|_2^2 > \frac{d_S^{2k}}{\ln(2)} \mathcal{J}_\mu(\delta)\right\} \\ = \mathbb{P}\left\{\|\Upsilon_B - \frac{\mathbb{1}}{d_S^{2k}}\|_2 > \frac{\mathcal{J}_\mu(\delta)}{d_B}\right\} \leq \mathcal{G}_\mu(\delta), \end{aligned} \quad (72)$$

where in the last line we have used Eq. (D1).  $\square$

This result says that repeated measurements of a typical process generated from random evolution gives maximal information. In other words, one only sees maximally noisy measurement results.

We have shown that Haar random evolution, as well as that generated by  $\epsilon$ -approximate  $t$ -designs, constitute mechanisms that are highly likely to produce chaos. This is clearly not the only internal mechanism that causes chaotic phenomena; c. f. Fig. 1 a). The next step will be to understand how a continuous quantum evolution, defined by time independent Hamiltonians, can lead to chaos.

For example, the so-called Wigner-Dyson level spacing distribution is often conflated with quantum chaos [3, 6]. This is the empirical observation that if one computes the distribution between next-neighbour energy levels, it follows a characteristic form when the semiclassical limit of the Hamiltonian is chaotic. An interesting connection may be found in entanglement spectra, which can be connected to a sense of irreversibility of a dynamics [84]. Another example is the eigenstate thermalisation hypothesis (ETH), which proposes that certain ‘physical’ observables look thermal according to individual eigenstates of

certain Hamiltonians. Often one calls such Hamiltonians chaotic, and the ETH leads to a deterministic (pure-state) foundation of statistical mechanics results.

It will be interesting to determine how (if) these mechanisms lead to a volume-law structure of spatiotemporal entanglement within a process; whether these are mechanisms of chaos. Indeed, such a connection would firmly cement quantum chaos as a foundational, deterministic principle underlying statistical mechanics, in perfect analogy with the classical case. Volume law entanglement of eigenstates is already a key feature of the strong ETH. In addition, for more specific Hamiltonian classes, Refs. [85, 86] determine that volume-law entanglement is highly typical. In this context, a key question will be how (many-body) quantum scars play into this, i.e. when some eigenstates of an apparently chaotic Hamiltonian do not satisfy the ETH. Such eigenstates can have different entanglement scaling [87–89].

Finally, the typicality bounds presented here have foundational implications regarding the prevalence of Markovianity in nature, which we will now discuss in our concluding remarks.

## VII. CONCLUSIONS

Starting from a theory-independent notion of chaos as the butterfly effect, in this work we have identified the underlying structure of quantum chaos (Section III), shown that it implies and hence unifies previous diagnostics (Section IV), given examples of quantum butterfly effect protocols (Section V), and lastly identified a number of mechanisms that lead to quantum chaos (Section VI). This framework is summarised in Fig. 1.

The results of Refs. [56, 57] state that processes generated from random dynamics are highly likely to be almost Markovian, for large enough systems. Paradoxically, Theorem 6 states that perturbations in such processes have a strong impact in the environment. That is, most random processes are chaotic. To make sense of this, note that Markovianity is with respect to a restricted measurement space, often taken to be small. Then, when a process is highly chaotic, a butterfly impacts the future pure state in such a strong and non-local way, that for any small subsystem it looks entirely noisy and hence Markovian on this future measurement space. Given that in nature chaos is the rule, not the exception, this helps address the fundamental question of why Markovian phenomena are so prevalent in nature [42, 43, 56, 57, 90]: chaotic processes on large systems look Markovian with respect to interventions on a much smaller subsystem. We anticipate that this may be a key factor in understanding the emergence of thermalisation from underlying quantum theory; in particular

the necessary loss of memory in the process of thermalisation. It would be interesting to investigate this further in a future work.

This is related to Refs. [91, 92], where it is shown that states which are too entangled - which is most states in the full Hilbert space - are not useful for measurement-based quantum computation. For such states which are too entangled, one can replace the local statistics with ‘coin flipping’ – purely classical stochasticity. It is, however, very difficult to produce large, highly entangled states. Usefulness is not proportional to the resources required to create a state. Our results in Section VI are a spatiotemporal version of this. Most processes are so chaotic, that future measurements statistics constitute purely classical noise. What is needed, then, to have complex, quantum non-Markovian phenomena? We propose that it is ‘between order and chaos’ where these interesting processes lie [93]. Within the framework we have laid out in this work, this would correspond to processes with sub-volume-law (logarithmic) spatiotemporal entanglement scaling. This is intrinsically tied to criticality in the spatial setting, and the MERA tensor network [52]. We are currently working on a concurrent project that explores a temporal version of the MERA network, structurally exhibiting long-range (polynomially decaying) temporal correlations [94].

A relevant problem which we have not tackled in this work is the question of how (if) classical chaos emerges from quantum chaos in some limit. While historically this was the main motivation for understanding quantum chaos [3, 5, 6], here we have developed a genuinely quantum notion of chaos, of interest for the wide range of phenomena and modern experiments with no classical analogue. It is therefore an open question how exactly to connect this to the classical picture. Modern notions of the transition to classicality may be integral to understanding this, such as quantum Darwinism [95] or classical stochasticity arising from quantum theory [44, 45, 90]. Related to this is Ref. [96], where it is shown that circuits generated solely by Clifford gates, or doped with only a few non-Clifford gates, are not chaotic according to a heuristic based off a generalised OTOC. It would be interesting to check what kind of entanglement structure a (doped) Clifford circuit has, that is whether this statement is consistent with the structure of chaos we have revealed in this work. This would have implications regarding whether any chaotic quantum process, as defined in Result 1, can be simulated classically.

The quantum butterfly effect was constructed in terms of a fidelity between final states. However, there may be another, more appropriate metric. Given the realisation of Result 1, one could concoct any such distance or diagnostic which probes the spatiotemporal entanglement structure of a process. One possibly interesting metric is that from Ref. [97]. There they define a class of geometric measures to the closest MPS of some constant bond dimension  $D$ . In the process setting, from Result 1 an equivalent concept would then correspond to the distance to the closest non-chaotic process. The utility of the principle of quantum chaos presented in this work is that it allows the understanding of the underlying cause of *any* chaos heuristic, and as a test of its validity. Beyond this, as discussed in Section IV E, using the framework stemming from Result 1, one can reinterpret and approach many problems and phenomena in many-body physics, such as Many-Body Localisation [73, 74], many-body quantum scars [98], and measurement induced phase transitions [75, 76], to name a few.

It is difficult to directly convert from classical to quantum chaos, due to the linearity of isolated quantum mechanics. The beauty of our approach is that it treats chaos itself as a primitive concept, independent of whether we adopt a classical or quantum formalism. Classically, this reduces to a non-linearity of the dynamics. On the quantum side of things, we have shown that spatiotemporal entanglement structure directly satisfies this principle: perturb a small part of a system in the past, and see a large, non-local effect in the future. From this realisation, we have shown that previous diagnostics fit perfectly within this framework - and in fact can be derived from it. Further, one can systematically address the validity of any quantum chaos diagnostic, and take a novel perspective in tackling a wide range of relevant problems in the field of many-body physics.

## ACKNOWLEDGMENTS

ND is supported by an Australian Government Research Training Program Scholarship and the Monash Graduate Excellence Scholarship. KM is supported through Australian Research Council Future Fellowship FT160100073, Discovery Project DP210100597, and the International Quantum U Tech Accelerator award by the US Air Force Research Laboratory.

- 
- [1] J. Kudler-Flam, L. Nie, and S. Ryu, Conformal field theory and the web of quantum chaos diagnostics, *Journal of High Energy Physics* **2020**, 175 (2020).
  - [2] A. Bhattacharyya, W. Chemsyany, S. S. Haque, and

- B. Yan, Towards the web of quantum chaos diagnostics, *European Physical Journal C: Particles and Fields* **82**, 10.1140/epjc/s10052-022-10035-3 (2022).
- [3] M. V. Berry, M. Tabor, and J. M. Ziman, Level cluster-



- ing in the regular spectrum, *Proceedings of the Royal Society of London. A. Mathematical and Physical Sciences* **356**, 375 (1977).
- [4] G. Lindblad, Quantum ergodicity and chaos, in *Fundamental Aspects of Quantum Theory*, edited by V. Gorini and A. Frigerio (Plenum Press, New York, 1986) p. 199.
  - [5] L. Reichl, *The Transition to Chaos: Conservative Classical and Quantum Systems*, Vol. 200 (Springer Nature, 2021).
  - [6] F. Haake, S. Gnutzmann, and M. Kuś, *Quantum Signatures of Chaos* (Springer, Cham, 2018).
  - [7] P. Hayden and J. Preskill, Black holes as mirrors: quantum information in random subsystems, *Journal of High Energy Physics* **2007**, 120 (2007).
  - [8] S. H. Shenker and D. Stanford, Black holes and the butterfly effect, *Journal of High Energy Physics* **2014**, 67 (2014).
  - [9] S. Popescu, A. J. Short, and A. Winter, Entanglement and the foundations of statistical mechanics, *Nat. Phys.* **2**, 754 (2006).
  - [10] C. Gogolin and J. Eisert, Equilibration, thermalisation, and the emergence of statistical mechanics in closed quantum systems, *Rep. Prog. Phys.* **79**, 056001 (2016).
  - [11] L. D'Alessio, Y. Kafri, A. Polkovnikov, and M. Rigol, From quantum chaos and eigenstate thermalization to statistical mechanics and thermodynamics, *Adv. Phys.* **65**, 239 (2016).
  - [12] A. Peres, Stability of quantum motion in chaotic and regular systems, *Phys. Rev. A* **30**, 1610 (1984).
  - [13] J. Emerson, Y. S. Weinstein, S. Lloyd, and D. G. Cory, Fidelity decay as an efficient indicator of quantum chaos, *Phys. Rev. Lett.* **89**, 284102 (2002).
  - [14] P. Pechukas, Kolmogorov entropy and quantum chaos, *The Journal of Physical Chemistry* **86**, 2239 (1982).
  - [15] W. Ślomczyński and K. Życzkowski, Quantum chaos: An entropy approach, *J. Math. Phys.* **35**, 5674 (1994).
  - [16] R. Alicki and M. Fannes, Defining quantum dynamical entropy, *Lett. Math. Phys.* **32**, 75 (1994).
  - [17] Alexei Kitaev, 2015 breakthrough prize fundamental physics symposium, URL: <https://breakthroughprize.org/Laureates/1/L3> (2014).
  - [18] J. Maldacena, S. H. Shenker, and D. Stanford, A bound on chaos, *Journal of High Energy Physics* **2016**, 106 (2016).
  - [19] B. Swingle, G. Bentsen, M. Schleier-Smith, and P. Hayden, Measuring the scrambling of quantum information, *Phys. Rev. A* **94**, 040302 (2016).
  - [20] M. Campisi and J. Goold, Thermodynamics of quantum information scrambling, *Phys. Rev. E* **95**, 062127 (2017).
  - [21] These three are some of the most popularly accepted chaos probes, but are by no means an exhaustive list. For example, two interesting alternative measures can be found in Refs. [84, 99]. Also see [1, 100] and references therein.
  - [22] J. M. Deutsch, Quantum statistical mechanics in a closed system, *Phys. Rev. A* **43**, 2046 (1991).
  - [23] M. Srednicki, Chaos and quantum thermalization, *Phys. Rev. E* **50**, 888 (1994).
  - [24] M. Rigol, V. Dunjko, and M. Olshanii, Thermalization and its mechanism for generic isolated quantum systems, *Nature* **452**, 854 EP (2008).
  - [25] B. Yan, L. Cincio, and W. H. Zurek, Information scrambling and loschmidt echo, *Phys. Rev. Lett.* **124**, 160603 (2020).
  - [26] D. A. Roberts and B. Yoshida, Chaos and complexity by design, *J. High Energy Phys.* **2017** (4), 121.
  - [27] L. Leone, S. F. E. Oliviero, and A. Hamma, Isospectral twirling and quantum chaos, *Entropy* **23** (2021).
  - [28] S. Milz and K. Modi, Quantum stochastic processes and quantum non-markovian phenomena, *PRX Quantum* **2**, 030201 (2021).
  - [29] J. C. Bridgeman and C. T. Chubb, Hand-waving and interpretive dance: an introductory course on tensor networks, *Journal of Physics A: Mathematical and Theoretical* **50**, 223001 (2017).
  - [30] R. Orús, A practical introduction to tensor networks: Matrix product states and projected entangled pair states, *Annals of Physics* **349**, 117 (2014).
  - [31] F. A. Pollock, C. Rodríguez-Rosario, T. Frauenheim, M. Paternostro, and K. Modi, Non-markovian quantum processes: Complete framework and efficient characterization, *Phys. Rev. A* **97**, 012127 (2018).
  - [32] J. Watrous, *The Theory of Quantum Information* (Cambridge University Press, 2018).
  - [33] F. A. Pollock, C. Rodríguez-Rosario, T. Frauenheim, M. Paternostro, and K. Modi, Operational markov condition for quantum processes, *Phys. Rev. Lett.* **120**, 040405 (2018).
  - [34] G. Chiribella, G. M. D'Ariano, and P. Perinotti, Quantum circuit architecture, *Phys. Rev. Lett.* **101**, 060401 (2008).
  - [35] G. Chiribella, G. M. D'Ariano, and P. Perinotti, Theoretical framework for quantum networks, *Phys. Rev. A* **80**, 022339 (2009).
  - [36] F. Costa and S. Shrapnel, Quantum causal modelling, *New J. Phys.* **18**, 063032 (2016).
  - [37] O. Oreshkov and C. Giarmatzis, Causal and causally separable processes, *New J. Phys.* **18**, 093020 (2016).
  - [38] M. A. Nielsen and I. L. Chuang, *Quantum Computation and Quantum Information: 10th Anniversary Edition* (Cambridge University Press, 2010).
  - [39] S. Shrapnel, F. Costa, and G. Milburn, Updating the born rule, *New J. Phys.* **20**, 053010 (2018).
  - [40] P. Taranto, F. A. Pollock, S. Milz, M. Tomamichel, and K. Modi, Quantum markov order, *Phys. Rev. Lett.* **122**, 140401 (2019).
  - [41] P. Taranto, S. Milz, F. A. Pollock, and K. Modi, Structure of quantum stochastic processes with finite markov order, *Phys. Rev. A* **99**, 042108 (2019).
  - [42] N. Dowling, P. Figueroa-Romero, F. A. Pollock, P. Strasberg, and K. Modi, Relaxation of multitime statistics in quantum systems (2021), [arXiv:2108.07420 \[quant-ph\]](https://arxiv.org/abs/2108.07420).
  - [43] N. Dowling, P. Figueroa-Romero, F. Pollock, P. Strasberg, and K. Modi, Equilibration of non-markovian quantum processes in finite time intervals (2021), [arXiv:2112.01099 \[quant-ph\]](https://arxiv.org/abs/2112.01099).
  - [44] P. Strasberg and M. G. Díaz, Classical quantum stochastic processes, *Phys. Rev. A* **100**, 022120 (2019).
  - [45] S. Milz, D. Egloff, P. Taranto, T. Theurer, M. B. Plenio, A. Smirne, and S. F. Huelga, When is a non-markovian quantum process classical?, *Phys. Rev. X* **10**, 041049 (2020).
  - [46] S. Milz, C. Spee, Z.-P. Xu, F. A. Pollock, K. Modi, and O. Gühne, Genuine Multipartite Entanglement in Time, *SciPost Phys.* **10**, 141 (2021).
  - [47] G. A. L. White, F. A. Pollock, L. C. L. Hollenberg,

- C. D. Hill, and K. Modi, From many-body to many-time physics (2021).
- [48] M. Fannes, B. Nachtergaele, and R. F. Werner, Finitely correlated states on quantum spin chains, *Communications in Mathematical Physics* **144**, 443 (1992).
- [49] J. Eisert, M. Cramer, and M. B. Plenio, Colloquium: Area laws for the entanglement entropy, *Reviews of modern physics* **82**, 277–306 (2010).
- [50] G. Vidal, J. I. Latorre, E. Rico, and A. Kitaev, Entanglement in quantum critical phenomena, *Phys. Rev. Lett.* **90**, 227902 (2003).
- [51] A. Nahum, S. Vijay, and J. Haah, Operator spreading in random unitary circuits, *Physical Review X* **8**, 021014 (2018).
- [52] G. Vidal, Entanglement renormalization, *Phys. Rev. Lett.* **99**, 220405 (2007).
- [53] C. Schön, E. Solano, F. Verstraete, J. I. Cirac, and M. M. Wolf, Sequential generation of entangled multiqubit states, *Phys. Rev. Lett.* **95**, 110503 (2005).
- [54] S.-J. Ran, Encoding of matrix product states into quantum circuits of one- and two-qubit gates, *Physical review. A* **101**, 032310 (2020).
- [55] E. Lorenz, *Predictability: does the flap of a butterfly's wing in Brazil set off a tornado in Texas?* (1972).
- [56] P. Figueroa-Romero, K. Modi, and F. A. Pollock, Almost markovian processes from closed dynamics, *Quantum* **3**, 136 (2019).
- [57] P. Figueroa-Romero, F. A. Pollock, and K. Modi, Markovianization with approximate unitary designs, *Communications Physics* **4**, 1–11 (2021).
- [58] This quantity is alternatively called fidelity decay or Loschmidt Echo in the literature. We take the middle ground here, to give credit to the historical role of Peres [12], while remaining familiar to those who recognise this quantity as the latter.
- [59] D. Poulin, R. Blume-Kohout, R. Laflamme, and H. Ollivier, Exponential speedup with a single bit of quantum information: measuring the average fidelity decay, *Physical review letters* **92**, 177906 (2004).
- [60] A. M. Childs, Y. Su, M. C. Tran, N. Wiebe, and S. Zhu, Theory of trotter error with commutator scaling, *Phys. Rev. X* **11**, 011020 (2021).
- [61] S. Pilatowsky-Cameo, J. Chávez-Carlos, M. A. Bastarrachea-Magnani, P. Stránský, S. Lerma-Hernández, L. F. Santos, and J. G. Hirsch, Positive quantum lyapunov exponents in experimental systems with a regular classical limit, *Phys. Rev. E* **101**, 010202 (2020).
- [62] K. Hashimoto, K.-B. Huh, K.-Y. Kim, and R. Watanabe, Exponential growth of out-of-time-order correlator without chaos: inverted harmonic oscillator, *Journal of High Energy Physics* **2020**, 68 (2020).
- [63] T. Xu, T. Scaffidi, and X. Cao, Does scrambling equal chaos?, *Phys. Rev. Lett.* **124**, 140602 (2020).
- [64] S. Pappalardi, A. Russomanno, B. Žunković, F. Iemini, A. Silva, and R. Fazio, Scrambling and entanglement spreading in long-range spin chains, *Phys. Rev. B* **98**, 134303 (2018).
- [65] A. W. Harrow, L. Kong, Z.-W. Liu, S. Mehraban, and P. W. Shor, Separation of out-of-time-ordered correlation and entanglement, *PRX Quantum* **2**, 020339 (2021).
- [66] M. Zonnios, J. Levinsen, M. M. Parish, F. A. Pollock, and K. Modi, Signatures of quantum chaos in an out-of-time-order tensor, *Phys. Rev. Lett.* **128**, 150601 (2022).
- [67] G. Lindblad, Non-Markovian quantum stochastic processes and their entropy, *Commun. Math. Phys.* **65**, 281 (1979).
- [68] J. Cotler, C.-M. Jian, X.-L. Qi, and F. Wilczek, Superdensity operators for spacetime quantum mechanics, *J. High Energy Phys.* **2018** (9), 93.
- [69] S. Milz, F. Sakuldee, F. A. Pollock, and K. Modi, Kolmogorov extension theorem for (quantum) causal modelling and general probabilistic theories, *Quantum* **4**, 255 (2020).
- [70] D. Burgarth, P. Facchi, M. Ligabò, and D. Lonigro, Hidden non-markovianity in open quantum systems, *Phys. Rev. A* **103**, 012203 (2021).
- [71] M. Heyl, P. Hauke, and P. Zoller, Quantum localization bounds trotter errors in digital quantum simulation, *Science advances* **5**, eaau8342 (2019).
- [72] M. Santhanam, S. Paul, and J. B. Kannan, Quantum kicked rotor and its variants: Chaos, localization and beyond, *Physics Reports* **956**, 1 (2022), quantum kicked rotor and its variants: Chaos, localization and beyond.
- [73] F. Alet and N. Laflorencie, Many-body localization: An introduction and selected topics, *Comptes Rendus Physique* **19**, 498 (2018), quantum simulation / Simulation quantique.
- [74] S. D. Geraedts, R. Nandkishore, and N. Regnault, Many-body localization and thermalization: Insights from the entanglement spectrum, *Physical review. B, Condensed matter* **93**, 174202 (2016).
- [75] B. Skinner, J. Ruhman, and A. Nahum, Measurement-induced phase transitions in the dynamics of entanglement, *Phys. Rev. X* **9**, 031009 (2019).
- [76] L. Zhang, J. A. Reyes, S. Kourtis, C. Chamon, E. R. Mucciolo, and A. E. Ruckenstein, Nonuniversal entanglement level statistics in projection-driven quantum circuits, *Phys. Rev. B* **101**, 235104 (2020).
- [77] For a two level system, in the computational basis the plus-minus basis corresponds to
- $$|\pm\rangle = \frac{1}{\sqrt{2}}(|0\rangle \pm |1\rangle).$$
- [78] P. Hayden, D. W. Leung, and A. Winter, Aspects of generic entanglement, *Communications in Mathematical Physics* **265**, 95 (2006).
- [79] A. Harrow, P. Hayden, and D. Leung, Superdense coding of quantum states, *Phys. Rev. Lett.* **92**, 187901 (2004).
- [80] M. Brenes, S. Pappalardi, J. Goold, and A. Silva, Multipartite entanglement structure in the eigenstate thermalization hypothesis, *Phys. Rev. Lett.* **124**, 040605 (2020).
- [81] D. Poulin, A. Qarry, R. Somma, and F. Verstraete, Quantum simulation of time-dependent hamiltonians and the convenient illusion of hilbert space, *Phys. Rev. Lett.* **106**, 170501 (2011).
- [82] Y. Nakata, C. Hirche, M. Koashi, and A. Winter, Efficient quantum pseudorandomness with nearly time-independent hamiltonian dynamics, *Phys. Rev. X* **7**, 021006 (2017).
- [83] This states that for eigenvalues  $\lambda_\sigma$  of  $\sigma$  [101],

$$S(\rho||\sigma) \leq \frac{\|\rho - \sigma\|_1^2}{\ln(2)\min(\lambda_\sigma)} \quad (73)$$

- [84] C. Chamon, A. Hama, and E. R. Mucciolo, Emergent irreversibility and entanglement spectrum statistics, *Phys. Rev. Lett.* **112**, 240501 (2014).
- [85] L. Vidmar, L. Hackl, E. Bianchi, and M. Rigol, Volume law and quantum criticality in the entanglement entropy of excited eigenstates of the quantum ising model, *Physical review letters* **121**, 220602 (2018).
- [86] E. Bianchi, L. Hackl, M. Kieburg, M. Rigol, and L. Vidmar, Volume-law entanglement entropy of typical pure quantum states, *PRX Quantum* **3**, 10.1103/prxquantum.3.030201 (2022).
- [87] M. Serbyn, D. A. Abanin, and Z. Papić, Quantum many-body scars and weak breaking of ergodicity, *Nature physics* **17**, 675–685 (2021).
- [88] Z. Yao, L. Pan, S. Liu, and H. Zhai, Quantum many-body scars and quantum criticality, *Physical review. B, Condensed matter* **105**, 125123 (2022).
- [89] S. Moudgalya, B. A. Bernevig, and N. Regnault, Quantum many-body scars and hilbert space fragmentation: a review of exact results, *Reports on Progress in Physics* **85**, 10.1088/1361-6633/ac73a0 (2022).
- [90] P. Strasberg, A. Winter, J. Gemmer, and J. Wang, *Classicality, markovianity and local detailed balance from pure state dynamics* (2022).
- [91] M. J. Bremner, C. Mora, and A. Winter, Are random pure states useful for quantum computation?, *Physical review letters* **102**, 190502 (2009).
- [92] D. Gross, S. T. Flammia, and J. Eisert, Most quantum states are too entangled to be useful as computational resources, *Physical review letters* **102**, 190501 (2009).
- [93] J. P. Crutchfield, Between order and chaos, *Nature Physics* **8**, 17 (2012).
- [94] N. Dowling, I. Aloisio, K. Modi, and S. Singh, *In preparation* (2022).
- [95] W. H. Zurek, Decoherence, einselection, and the quantum origins of the classical, *Rev. Mod. Phys.* **75**, 715 (2003).
- [96] L. Leone, S. F. E. Oliviero, Y. Zhou, and A. Hama, Quantum Chaos is Quantum, *Quantum* **5**, 453 (2021).
- [97] A. Nico-Katz and S. Bose, *An entanglement-complexity generalization of the geometric entanglement* (2022).
- [98] N. S. Srivatsa, H. Yarloo, R. Moessner, and A. E. B. Nielsen, Mobility edges through inverted quantum many-body scarring, *arXiv preprint arXiv:2208.01054* (2022).
- [99] N. Anand, G. Styliaris, M. Kumari, and P. Zanardi, Quantum coherence as a signature of chaos, *Phys. Rev. Research* **3**, 023214 (2021).
- [100] N. Hunter-Jones, *Chaos and Randomness in Strongly-Interacting Quantum Systems*, *Ph.D. thesis*, California Institute of Technology (2018).
- [101] I. Sason, On reverse pinsker inequalities, *arXiv preprint arXiv:1503.07118* (2015).
- [102] Markov's inequality states that for any non-negative random variable  $X$  with mean  $\mathbb{E}(X)$ , and for any  $\delta > 0$ ,  $\mathbb{P}(X \geq \delta) \leq \mathbb{E}(X)/\delta$ .
- [103] R. A. Low, Large deviation bounds for k-designs, *Proceedings of the Royal Society A: Mathematical, Physical and Engineering Sciences* **465**, 3289–3308 (2009).
- [104] Instrument Choi states generally are supernormalised; see Eq. (11) and the surrounding discussion.

## Appendix A: Construction of Basis of Multitime Instruments

To construct a basis of unitary butterflies, one can do the following procedure:

1. Choose any orthonormal basis of unitary matrices  $\{\sigma_i^{(\ell)}\}_{i=1}^{d_S^2}$  for each time  $S(t_\ell)$ ,

$$\text{tr}[\sigma_i^{(\ell)} \sigma_j^{(\ell)}] = d_S \delta_{ij} \quad (\text{A1})$$

For example, this could be the generalised Pauli matrices [26].

2. Using single-time CJI, map these operators to states by having them act on half of a maximally entangled state on the doubled space  $\mathcal{H}_{S(t_\ell)} \otimes \mathcal{H}_{S(t_\ell)'}$ ,

$$|x_i^{(\ell)}\rangle := (\sigma_i^{(\ell)} \otimes \mathbb{1}) |\phi^+\rangle_{S(t_\ell)S'(t_\ell)}. \quad (\text{A2})$$

the orthonormality condition (A1) carries over to this representation,

$$\langle x_i^{(\ell)} | x_j^{(\ell)} \rangle = d_S \delta_{ij}. \quad (\text{A3})$$

3. Do this for every time to arrive at a full basis for the butterfly space  $\mathcal{H}_B \equiv \mathcal{H}_{S(t_k)}^o \otimes \mathcal{H}_{S(t_{k-1})}^{\text{io}} \cdots \otimes \mathcal{H}_{S(t_2)}^{\text{io}} \otimes \mathcal{H}_{S(t_1)}^{\text{io}}$ , together with some portion of the final state,  $\mathcal{H}_{\bar{R}}$ ,

$$\{|\tilde{x}_i^t\rangle\}_i^{d_{B\bar{R}}} := \left\{ |x_{i_0}^{(0)}\rangle \otimes |x_{i_1}^{(1)}\rangle \otimes \cdots \otimes |x_{i_k}^{(k)}\rangle \right\}_{i_0, i_1, \dots, i_k=1}^{d_R, d_S, \dots, d_S}$$

4. To make these a random basis, one can apply a global Haar random (or  $t$ -design) unitary to each element. This is relevant for Theorem 3.

## Appendix B: Proof of Theorem 3

We will use the following result, which we prove below using an application of Weingarten Calculus: for the Haar random sampling of two orthogonal projections  $\{|\tilde{x}\rangle, |\tilde{y}\rangle\}$ , the expectation value is

$$\begin{aligned} \mathbb{E}_{\mathcal{X} \sim \mathcal{H}} \left\{ \left( |\langle \tilde{y} | \Upsilon_{B\bar{R}} | \tilde{x} \rangle|^2 \right) \right\}_{\tilde{x} \perp \tilde{y}} &= \frac{d_{B\bar{R}}^2 (\text{tr}[\Upsilon_{B\bar{R}}^2] - 1/d_{B\bar{R}})}{d_{B\bar{R}}^2 - 1} \\ &\approx \text{tr}[\Upsilon_{B\bar{R}}^2] - 1/d_{B\bar{R}}, \end{aligned} \quad (\text{B1})$$

where we take  $d_{B\bar{R}}^2 - 1 \approx d_{B\bar{R}}^2$  in the second line.

*Proof.* Two Haar random, orthogonal states  $\{|\tilde{x}\rangle, |\tilde{y}\rangle\}_{\mathcal{H}}$  can be generated from any other, e.g. computational,

orthogonal states  $\{|0\rangle, |1\rangle\}$ , given a random unitary matrix  $U \in \mathcal{H}$ , by identifying  $|\tilde{x}\rangle = U|0\rangle$  and  $|\tilde{y}\rangle = U|1\rangle$ . Define  $\Phi_H^{(2)}(A)$  to be the 2-fold average of the tensor  $A \in \mathcal{H} \otimes \mathcal{H}$ . We may use Weingarten Calculus to compute it explicitly [26]

$$\begin{aligned} \Phi_H^{(2)}(A) &:= \int dU U \otimes U(A) U^\dagger \otimes U^\dagger \\ &= \frac{1}{d^2 - 1} \left( \mathbb{1} \operatorname{tr}[A] + \mathbb{S} \operatorname{tr}[SA] - \frac{1}{d} \mathbb{S} \operatorname{tr}[A] - \frac{1}{d} \mathbb{1} \operatorname{tr}[SA] \right), \end{aligned} \quad (\text{B2})$$

where  $\mathbb{S}$  is the swap operation. By choosing  $A \equiv \Upsilon_{B\bar{R}} \otimes \Upsilon_{B\bar{R}}$ , we can rewrite the left hand side of Eq. (B1) as

$$\begin{aligned} LHS &= \int dU_H \langle \tilde{x} | U \Upsilon_{B\bar{R}} U^\dagger | \tilde{y} \rangle \langle \tilde{y} | U \Upsilon_{B\bar{R}} U^\dagger | \tilde{x} \rangle \\ &= \langle \tilde{x} | \langle \tilde{y} | \left( \int dU_H U^{\otimes 2} (\Upsilon_{B\bar{R}} \otimes \Upsilon_{B\bar{R}}) U^{\dagger \otimes 2} \right) | \tilde{y} \rangle | \tilde{x} \rangle \\ &= \langle \tilde{x} | \langle \tilde{y} | \Phi_H^{(2)}(\Upsilon_{B\bar{R}} \otimes \Upsilon_{B\bar{R}}) | \tilde{y} \rangle | \tilde{x} \rangle \\ &= \langle \tilde{x} | \langle \tilde{y} | \left( \frac{1}{d_{B\bar{R}}^2 - 1} \left( \mathbb{1} \operatorname{tr}[\Upsilon_{B\bar{R}} \otimes \Upsilon_{B\bar{R}}] \right. \right. \\ &\quad \left. \left. + \mathbb{S} \operatorname{tr}[\mathbb{S}(\Upsilon_{B\bar{R}} \otimes \Upsilon_{B\bar{R}})] - \frac{1}{d_{B\bar{R}}} \mathbb{S} \operatorname{tr}[\Upsilon_{B\bar{R}} \otimes \Upsilon_{B\bar{R}}] \right. \right. \\ &\quad \left. \left. - \frac{1}{d_{B\bar{R}}} \mathbb{1} \operatorname{tr}[\mathbb{S}(\Upsilon_{B\bar{R}} \otimes \Upsilon_{B\bar{R}})] \right) | \tilde{y} \rangle | \tilde{x} \rangle. \end{aligned} \quad (\text{B3})$$

For the first trace in this equation, we can directly evaluate

$$\operatorname{tr}[\Upsilon_{B\bar{R}} \otimes \Upsilon_{B\bar{R}}] = \operatorname{tr}[\Upsilon_{B\bar{R}}]^2 = 1 \quad (\text{B4})$$

For the second trace,

$$\operatorname{tr}[\mathbb{S}(\Upsilon_{B\bar{R}} \otimes \Upsilon_{B\bar{R}})] = \operatorname{tr}(\Upsilon_{B\bar{R}}^2). \quad (\text{B5})$$

Then, by the orthogonality of the butterflies,  $\langle \tilde{x} | \langle \tilde{y} | \mathbb{1} | \tilde{y} \rangle | \tilde{x} \rangle = 0$  while  $\langle \tilde{x} | \langle \tilde{y} | \mathbb{S} | \tilde{y} \rangle | \tilde{x} \rangle = d_{B\bar{R}}^2$ , and so only the second and third terms in the final line of (B3) survive. Using this, we arrive at Eq. (B1).  $\square$

We will now use this to prove Theorem 3.

For part **A** of the theorem, we can directly apply this to Markov's inequality,<sup>[102]</sup>

$$\begin{aligned} \mathbb{P}_{\mathcal{X} \sim \mathcal{H}} \left\{ \tilde{\zeta}(\Upsilon, \mathcal{X}) \geq \delta \right\} &= \mathbb{P} \left\{ \sup_{\tilde{R}} \left( |\langle \tilde{y} | \Upsilon_{B\bar{R}} | \tilde{x} \rangle|^2 \right) \geq \delta \right\} \\ &\leq \frac{\mathbb{E}_{\mathcal{X} \sim \mathcal{H}} \left\{ |\langle \tilde{y} | \Upsilon_{B\bar{R}} | \tilde{x} \rangle|^2 \right\}}{\delta} \\ &\approx \frac{\operatorname{tr}[\Upsilon_{B\bar{R}}^2] - 1/(d_{B\bar{R}})}{\delta}. \end{aligned} \quad (\text{B6})$$

For the proof of part **B** of the theorem, we will again use Eq. (B1), given that this equation is independent of

the particular choice of orthogonal  $|\tilde{x}\rangle$  and  $|\tilde{y}\rangle$  and is invariant over an average of many butterflies  $|\tilde{x}_i\rangle$ ,

$$\mathbb{E}_{\mathcal{X} \sim \mathcal{H}} \left\{ \left( \frac{1}{d_{B\bar{R}}^2 - d_{B\bar{R}}} \sum_{i \neq j} |\langle \tilde{x}_i | \Upsilon_{B\bar{R}} | \tilde{x}_j \rangle|^2 \right) \right\} \quad (\text{B7})$$

$$= \frac{1}{d_{B\bar{R}}^2 - d_{B\bar{R}}} \sum_{i \neq j} \mathbb{E}_{\mathcal{X} \sim \mathcal{H}} \left\{ \left( |\langle \tilde{x}_1 | \Upsilon_{B\bar{R}} | \tilde{x}_2 \rangle|^2 \right) \right\} \quad (\text{B8})$$

$$= \mathbb{E}_{\mathcal{X} \sim \mathcal{H}} \left\{ \left( |\langle \tilde{x}_1 | \Upsilon_{B\bar{R}} | \tilde{x}_2 \rangle|^2 \right) \right\} \quad (\text{B9})$$

We will now apply this to the reverse Markov inequality, which states that for  $\delta < \mathbb{E}\{X\}$  and  $\mathbb{P}\{X \leq a\} = 1$ ,

$$\mathbb{P}\{X > \delta\} \geq \frac{\mathbb{E}\{X\} - \delta}{a - \delta}. \quad (\text{B10})$$

We define  $a$  as follows,

$$\begin{aligned} a &:= \frac{1}{1 - 1/(d_{B\bar{R}})} \operatorname{tr}[\Upsilon_{B\bar{R}}^2] \\ &= \frac{d_{B\bar{R}}^2}{d_{B\bar{R}}^2 - d_{B\bar{R}}} \sum_{i,j} |(\Upsilon_{B\bar{R}})_{ij}|^2 \\ &= \frac{1}{d_{B\bar{R}}^2 - d_{B\bar{R}}} \sum_{i,j} |\langle \tilde{x}_i | \Upsilon_{B\bar{R}} | \tilde{x}_j \rangle|^2 \end{aligned} \quad (\text{B11})$$

$$\begin{aligned} &\geq \frac{1}{d_{B\bar{R}}^2 - d_{B\bar{R}}} \sum_{i \neq j} |\langle \tilde{x}_i | \Upsilon_{B\bar{R}} | \tilde{x}_j \rangle|^2 \\ &= \tilde{\zeta}(\Upsilon, \mathcal{X}_b) \end{aligned} \quad (\text{B12})$$

where we have used that the projectors  $|\tilde{x}_i\rangle$  correspond to unitary instruments and so have normalisation  $d_{B\bar{R}}$ ; see Eq. (11). This choice of  $a$  then satisfies

$$\mathbb{P} \left\{ \frac{1}{d_{B\bar{R}}^2 - d_{B\bar{R}}} \sum_{i \neq j} |\langle \tilde{x}_i | \Upsilon_{B\bar{R}} | \tilde{x}_j \rangle|^2 \leq a \right\} = 1. \quad (\text{B13})$$

Applying Eq. (B1) to the reverse Markov inequality (B10), we arrive at

$$\begin{aligned} &\mathbb{P}\{\tilde{\zeta}(\Upsilon, \mathcal{X}_b) > \delta\} \\ &\geq \frac{\mathbb{E}_{\mathcal{X} \sim \mathcal{H}} \left\{ \left( \frac{1}{d_{B\bar{R}}^2 - d_{B\bar{R}}} \sum_{i \neq j} |\langle \tilde{x}_i | \Upsilon_{B\bar{R}} | \tilde{x}_j \rangle|^2 \right) \right\} - \delta}{\frac{1}{1 - 1/(d_{B\bar{R}})} \operatorname{tr}[\Upsilon_{B\bar{R}}^2] - \delta} \\ &\geq \frac{\operatorname{tr}[\Upsilon_{B\bar{R}}^2] - 1/d_{B\bar{R}} - \delta}{\frac{1}{1 - 1/(d_{B\bar{R}})} \operatorname{tr}[\Upsilon_{B\bar{R}}^2] - \delta} \end{aligned} \quad (\text{B14})$$

and where  $\delta$  can be chosen such that  $0 < \delta < \operatorname{tr}[\Upsilon_{B\bar{R}}^2] - 1/d_{B\bar{R}}$ . Without the large butterfly approximation, we choose

$$\delta = \frac{\operatorname{tr}[\Upsilon_{B\bar{R}}^2] d_{B\bar{R}}^2}{2(d_{B\bar{R}}^2 - 1)}, \quad (\text{B15})$$

and after some straightforward algebra we arrive at Eq. (50).



Finally, we only use the 2-fold channel in this proof, i.e. the second moment of the unitary Haar group. So by definition this result holds equally well if the butterflies are not completely Haar random, and are instead generated by a 2-design circuit.  $\square$

### Appendix C: Proof of Theorem 4

For either case of volume or area-law states, we can compute

$$\begin{aligned}
\langle \tilde{x}_i^\sigma | \Upsilon_{B\bar{R}} | \tilde{x}_j^\omega \rangle &= \langle \tilde{x}_i^\sigma | \sum_n \lambda_n | \alpha_n \rangle \langle \alpha_n | \tilde{x}_j^\omega \rangle \\
&= \frac{\sqrt{d_{B\bar{R}}}}{\sqrt{2}} (\langle \alpha_i | + \sigma \langle \alpha_{\bar{i}} |) \left( \sum_{n=1}^{d/2} \lambda_n | \alpha_n \rangle \langle \alpha_n | \right. \\
&\quad \left. + \sum_{n=1}^{d/2} \lambda_{d/2+n} | \alpha_{\bar{n}} \rangle \langle \alpha_{\bar{n}} | \right) \frac{\sqrt{d_{B\bar{R}}}}{\sqrt{2}} (| \alpha_j \rangle + \omega | \alpha_{\bar{j}} \rangle) \\
&= \frac{(\lambda_i + \sigma \omega \lambda_j)}{2} \delta_{ij} d_{B\bar{R}} \quad (C1)
\end{aligned}$$

where  $\lambda_{d/2+n} \equiv 0$  for area law,  $\chi = D \leq d_{B\bar{R}}/2$ , and  $\lambda_{d/2+n}$  are simply Schmidt coefficients for volume law,  $\chi = d_{B\bar{R}}$ . Using this, we see a qualitative difference in the behaviour of  $\tilde{\zeta}(\Upsilon, \mathcal{X})$  between area and volume-law states. First

$$\begin{aligned}
\tilde{\zeta}(\Upsilon^{(\text{ar})}, \mathcal{X}_{\text{sch}}) &= \frac{1}{d_{B\bar{R}}^2 - d_{B\bar{R}}} \sum_{\{i,\sigma\} \neq \{j,\omega\}}^{d_{B\bar{R}}^2 - d_{B\bar{R}}} \frac{|\langle x_i^\sigma | \Upsilon_{B\bar{R}}^{(\text{ar})} | x_j^\omega \rangle|^2}{\langle x_i^\sigma | \Upsilon_{B\bar{R}}^{(\text{ar})} | x_i^\sigma \rangle \langle x_j^\omega | \Upsilon_{B\bar{R}}^{(\text{ar})} | x_j^\omega \rangle} \\
&= \frac{1}{d_{B\bar{R}}^2 - d_{B\bar{R}}} \sum_{\{i,\sigma\} \neq \{j,\omega\}}^{d_{B\bar{R}}^2 - d_{B\bar{R}}} \frac{\frac{\lambda_i^2}{4} \delta_{ij}}{\frac{\lambda_i}{2} \frac{\lambda_j}{2}} \quad (C2) \\
&= \frac{1}{d_{B\bar{R}}^2 - d_{B\bar{R}}} \sum_{i=j, \sigma \neq \omega}^{D, 2} \frac{(\lambda_i/2)^2}{(\lambda_i/2)^2} \\
&= \frac{1}{d_{B\bar{R}}^2 - d_{B\bar{R}}} \sum_{\sigma \neq \omega = \pm 1} D = \frac{2D}{d_{B\bar{R}}^2 - d_{B\bar{R}}}.
\end{aligned}$$

For the volume-law upper-bound, we can again directly

apply Eq. (C1) to get

$$\begin{aligned}
\tilde{\zeta}(\Upsilon^{(\text{vol})}, \mathcal{X}_{\text{sch}}) &= \frac{1}{d_{B\bar{R}}^2 - d_{B\bar{R}}} \sum_{\{i,\sigma\} \neq \{j,\omega\}}^{d_{B\bar{R}}^2 - d_{B\bar{R}}} \frac{|\langle x_i^\sigma | \Upsilon_{B\bar{R}}^{(\text{vol})} | x_j^\omega \rangle|^2}{\langle x_i^\sigma | \Upsilon_{B\bar{R}}^{(\text{vol})} | x_i^\sigma \rangle \langle x_j^\omega | \Upsilon_{B\bar{R}}^{(\text{vol})} | x_j^\omega \rangle} \\
&= \frac{1}{d_{B\bar{R}}^2 - d_{B\bar{R}}} \sum_{\{i,\sigma\} \neq \{j,\omega\}}^{d_{B\bar{R}}^2 - d_{B\bar{R}}} \frac{\left( \frac{|\lambda_i + \sigma \omega \lambda_j|}{2} \right)^2 \delta_{ij}}{\frac{\lambda_i + \lambda_{\bar{i}}}{2} \frac{\lambda_j + \lambda_{\bar{j}}}{2}} \\
&= \frac{1}{d_{B\bar{R}}^2 - d_{B\bar{R}}} \sum_{i=j, \sigma \neq \omega}^{d_{B\bar{R}}} \frac{|\lambda_i - \lambda_{\bar{i}}|^2}{|\lambda_i + \lambda_{\bar{i}}|^2} \quad (C3) \\
&= \frac{2}{d_{B\bar{R}}^2 - d_{B\bar{R}}} \sum_i^{d_{B\bar{R}}/2} \frac{|\lambda_i - \lambda_{\bar{i}}|^2}{|\lambda_i + \lambda_{\bar{i}}|^2} \\
&\leq \frac{\Delta^2}{4(d_{B\bar{R}} - 1)\lambda_{\min}^2}
\end{aligned}$$

where in the final line we have defined the maximum spectral gap as in Theorem 4.

From the penultimate line of Eq. (C3), we can alternatively lower bound this quantity via

$$\begin{aligned}
\tilde{\zeta}(\Upsilon^{(\text{vol})}, \mathcal{X}_{\text{sch}}) &= \frac{2}{d_{B\bar{R}}^2 - d_{B\bar{R}}} \sum_i^{d/2} \frac{|\lambda_i - \lambda_{\bar{i}}|^2}{|\lambda_i + \lambda_{\bar{i}}|^2} \\
&\geq \frac{2}{d_{B\bar{R}}^2 - d_{B\bar{R}}} \sum_i^{d/2} \frac{|\lambda_i - \lambda_{\bar{i}}|}{|\lambda_i + \lambda_{\bar{i}}|} \\
&= \frac{2}{d_{B\bar{R}}^2 - d_{B\bar{R}}} \sum_{i,j}^d \frac{|\lambda_i - \lambda_j|^2}{|\lambda_i + \lambda_j|^2} \sum_{n=1}^{d/2} \delta_{in} \delta_{j(d/2+n)} \\
&= 2 \sum_{i,j}^d \frac{|\lambda_i - \lambda_j|^2}{|\lambda_i + \lambda_j|^2} \langle \alpha_i | X | \alpha_j \rangle \quad (C4) \\
&= \text{QFI}(\Upsilon^{(\text{vol})}, X)
\end{aligned}$$

where the inequality is due to the fact that  $|\lambda_i + \lambda_{\bar{i}}| < 1$ .  $\square$

### Appendix D: Typical Quantum Processes

Here we explain and utilise the main results from Refs. [56, 57], to prove concentration of measure bounds for typical processes. These results state that processes generated from random evolution – be it fully Haar random or from an  $\epsilon$ -approximate  $t$ -design – are likely to look Markovian when one only has access to repeated measurements on a small subsystem compared to the full unitarily evolving isolated system. We will modify these results to arrive at the following bound,

$$\mathbb{P}_{U_i \sim \mu} \left\{ \left\| \Upsilon_{B\bar{R}} - \frac{\mathbb{1}}{d_{B\bar{R}}} \right\|_2^2 \geq \frac{\mathcal{J}_\mu(\delta)}{d_{B\bar{R}}} \right\} \leq \mathcal{G}_\mu(\delta). \quad (D1)$$

## I. Process From Haar Random Evolution

For dynamics generated by independent Haar random unitaries, given that  $d_{B\bar{R}} = d_S^{2k} d_{\bar{R}} \approx d_S^{2k+1} < d_E \approx d_R$ , the Haar average of the left hand side of the inequality within the brackets of Eq. (D1) is

$$\begin{aligned} \mathbb{E}_H(\|\Upsilon_{B\bar{R}} - \frac{\mathbb{1}_{B\bar{R}}}{d_{B\bar{R}}}\|_2^2) &= \mathbb{E}_H(\text{tr}(\Upsilon_{B\bar{R}}^2)) - \frac{1}{d_{B\bar{R}}} \\ &= \frac{d_E^2 - 1}{d_E(d_{SE} + 11)} \left( \frac{d_E^2 - 1}{d_{SE}^2 - 1} \right)^k + \frac{1}{d_E} - \frac{1}{d_S^{2k+1}} \\ &=: \mathcal{B} \end{aligned} \quad (\text{D2})$$

This is proven in the Appendix F in Ref. [56]. Our setup is, however, a slightly modified version of this, as our final intervention is size  $d_{\bar{R}}$  rather than  $d_S$ . In detail, as  $\bar{R}$  is the final intervention space, one can modify the result Eq. (D2) by changing the factors  $\mathcal{A}$  and  $\mathcal{B}$  in Eq. (74) in Ref. [56] to,

$$\begin{aligned} \mathcal{A} &\rightarrow d_{SE} d_{\bar{R}^c} (d_{\bar{R}^c}^2 + d_{\bar{R}}^2 - 2), \text{ and} \\ \mathcal{B} &\rightarrow d_{SE} d_{\bar{R}^c} (d_{SE}^2 - 1) \end{aligned} \quad (\text{D3})$$

where  $\bar{R}^c$  is the complement to  $\bar{R}$ , such that  $\bar{R} \cup \bar{R}^c = R$ . Using this to simplify Eq. (74) in [56], we arrive a long, messy expression. However, it has same asymptotic behaviour as Eq. (D2). More precisely, we make the approximation that  $d_{\bar{R}} \approx d_S \ll d_E$  – which is valid for the usual butterfly assumption that  $d_{\bar{R}} \ll d_R$ .

In particular, if  $d_E \gg 1$ , such that  $d_E - 1 \approx d_E$ , then in both cases

$$\mathbb{E}_H(\|\Upsilon_{B\bar{R}} - \frac{\mathbb{1}_{B\bar{R}}}{d_{B\bar{R}}}\|_2^2) \approx \frac{1}{d_E}. \quad (\text{D4})$$

Now, using Levy's Lemma one can arrive at the following concentration of measure result [9]. For some probability measure  $\sigma$ , and function  $f(x)$  with  $\delta > 0$

$$\mathbb{P}_{x \sim \sigma} \{f(x) \geq \mathbb{E}_\sigma(f) + \delta\} \leq \alpha_\sigma(\delta/L), \quad (\text{D5})$$

where  $L > 0$  is the Lipschitz constant of  $f$ , which dictates how slowly varying  $f$  is in the measure space  $\sigma$ . The function  $\alpha_\sigma$  is the concentration rate, which we require to be vanishing in increasing  $\delta$  to describe a concentration of measure. For our situation this will be the exponential function

$$\exp\left(\frac{-\delta^2(k+1)d}{4L^2}\right) \quad (\text{D6})$$

which is proven in the Appendices of Ref. [56]. Now, the Lipschitz constants can also be bounded by almost the same quantity as in [56], despite here having  $f := \|\rho - \mathbb{1}/d\|_2^2$  compared to  $(1/2)\|\rho - \mathbb{1}/d\|_1$ . This is because we can use that  $\|X\|_2^2 \leq \|X\|_2 \leq \|X\|_1$ , where we also have

an additional factor of 2 in  $L$ , given the  $(1/2)$  factor in the definition of non-Markovianity  $\mathcal{N}$  in [56]. We therefore arrive at the Lemma

$$\mathbb{P}\left\{\|\Upsilon_{B\bar{R}} - \frac{\mathbb{1}_{B\bar{R}}}{d_{B\bar{R}}}\|_2^2 > \mathcal{B} + \delta\right\} \leq \exp[-C\delta^2] \quad (\text{D7})$$

for  $\mathcal{B}$  defined in Eq. (D2), and

$$\begin{aligned} \mathcal{C} &:= \frac{(k+1)d_E d_S (d_S - 1)^2}{8(d_S^{k+1} - 1)^2} \\ &= \frac{(k+1)d_E d_S}{8(d_S^k + d_S^{k-1} + \dots + 1)^2} \end{aligned} \quad (\text{D8})$$

defined from considerations above. Again, we have taken the approximation that  $d_{\bar{R}} \approx d_S$ .

## II. Process From $\epsilon$ -approximate unitary $t$ -designs

Now, for the  $t$ -design result, we adapt the results from Ref. [57], which in turn builds on the deviation bounds for  $k$ -design results of Ref. [103]. The concentration of measure takes the form

$$\mathcal{F} := \left\{ \left[ \frac{16m}{(k+1)d_{SE}} \left( \frac{d_S^{k+1} - 1}{d_S - 1} \right)^2 \right]^m + (\mathcal{B})^m \right\} \quad (\text{D9})$$

$$+ \frac{\epsilon}{16^m d_{SE}^t} \left( d_E^4 d_S^{2(k+2)} + \frac{1}{d_S^{2k+1}} \right), \quad (\text{D10})$$

For any  $0 < m \leq t/4$ , and  $\delta > 0$ .  $m$  can be chosen to optimise this bound, and overall  $\mathcal{F}$  is small for  $d_E \gg d_S^{2k+1} = d_{B\bar{R}}$ , for a high  $t$ . See Ref. [57] for details; a proof for this can be found in the methods section. Here we have slightly modified that result, as our object of interest is  $\|\Upsilon_{B\bar{R}} - \frac{\mathbb{1}_{B\bar{R}}}{d_{B\bar{R}}}\|_2^2$  rather than a non-Markovianity measure. This means we replace  $\mathcal{N}_\bullet \rightarrow \|\Upsilon_{B\bar{R}} - \frac{\mathbb{1}_{B\bar{R}}}{d_{B\bar{R}}}\|_2^2$  and  $\delta \rightarrow \sqrt{\delta}/2$ , and do not have the  $d_S^{3(2k+1)}$  factor on the right hand side of theorem 1 of Ref. [57]. In addition, we have a similar approximation as that considered above in Section D I, in that we take  $d_{\bar{R}} \approx d_S$ , valid for the asymptotic case where  $d_E \gg d_{\bar{R}}$ .

## III. Proof of Theorem 6

We will now utilise Eq. (D1) to prove that most random processes are chaotic.

Given the basis  $\{|\tilde{x}_i\rangle\}$ , define the (normalised) dephased state with respect to this,

$$D(\Upsilon_{B\bar{R}}) := \frac{1}{d_{B\bar{R}}^2} \sum_i^{d_{B\bar{R}}} (|\tilde{x}_i\rangle\langle\tilde{x}_i|) \Upsilon_B(|\tilde{x}_i\rangle\langle\tilde{x}_i|) \quad (\text{D11})$$

with diagonal elements  $\frac{1+a_i}{d_{B\bar{R}}}$  and  $\mu := \min_i |a_i|$ . Then, we will use the following inequality,

$$\begin{aligned} \|\Upsilon_{B\bar{R}} - \frac{\mathbb{1}}{d_{B\bar{R}}}\|_2 &\geq \frac{1}{\sqrt{d_{B\bar{R}}}} \|\Upsilon_{B\bar{R}} - \frac{\mathbb{1}}{d_{B\bar{R}}}\|_1 \\ &\geq \frac{1}{\sqrt{d_{B\bar{R}}}} \|D(\Upsilon_{B\bar{R}}) - \frac{\mathbb{1}}{d_{B\bar{R}}}\|_1 \\ &= \frac{1}{\sqrt{d_{B\bar{R}}}} \sum_i \left| \frac{a_i}{d_{B\bar{R}}} \right| \quad (\text{D12}) \\ &\geq \frac{1}{\sqrt{d_{B\bar{R}}}} d_{B\bar{R}} \frac{\mu}{d_{B\bar{R}}} \\ &= \frac{\mu}{\sqrt{d_{B\bar{R}}}}, \end{aligned}$$

where in the first line we have used that  $\|X\|_2 \geq$

$(1/\sqrt{d})\|X\|_1$ , and in the second we have used that dephasing, as a CPTP map, may not increase distinguishability between quantum states (monotonicity). Now,

$$\begin{aligned} \sum_{i \neq j} |(\Upsilon_{B\bar{R}})_{ij}|^2 &= \sum_{i \neq j} \left| \left( \Upsilon_{B\bar{R}} - \frac{\mathbb{1}}{d_{B\bar{R}}} \right)_{ij} \right|^2 \\ &\leq \sum_{i,j} \left| \left( \Upsilon_{B\bar{R}} - \frac{\mathbb{1}}{d_{B\bar{R}}} \right)_{ij} \right|^2 \quad (\text{D13}) \\ &= \left\| \Upsilon_{B\bar{R}} - \frac{\mathbb{1}}{d_{B\bar{R}}} \right\|_2^2, \end{aligned}$$

where in the first line we have used that for  $i \neq j$ ,  $\mathbb{1}_{ij} = 0$ , and in the second line we have included the extra positive terms in the sum where  $i = j$ .

We are now in a position to prove Theorem 6. We will drop the measure specification simply for economy of notation:  $\mathbb{P}_{U_i \sim \mu} \rightarrow \mathbb{P}$ .

Now, immediately cancelling the averaging normalization  $1/(d_{B\bar{R}}^2 - d_{B\bar{R}})$ , noting that  $\langle \tilde{x}_i | \Upsilon_{B\bar{R}} | \tilde{x}_j \rangle = d_{B\bar{R}}(\Upsilon_{B\bar{R}})_{ij}$ ,<sup>[104]</sup> and that  $\min_n ((\Upsilon_{B\bar{R}})_{nn}) = \frac{1-\mu}{d_{B\bar{R}}}$ , we arrive at

$$\begin{aligned} \mathbb{P}\left\{ \tilde{\zeta}(\Upsilon, \mathcal{X}_b) \geq \frac{\mathcal{J}_\mu(\delta)}{(d_{B\bar{R}} - 1)(1 - \sqrt{\mathcal{J}_\mu(\delta)})^2} \right\} &= \mathbb{P}\left\{ \sum_{i \neq j} \frac{(\Upsilon_{B\bar{R}})_{ij}^2}{(\Upsilon_{B\bar{R}})_{ii}(\Upsilon_{B\bar{R}})_{jj}} \geq \frac{d_{B\bar{R}}\mathcal{J}_\mu(\delta)}{(1 - \sqrt{\mathcal{J}_\mu(\delta)})^2} \right\} \\ &\leq \mathbb{P}\left\{ \frac{\sum_{i \neq j} (\Upsilon_{B\bar{R}})_{ij}^2}{\min_n (\Upsilon_{B\bar{R}})_{nn}^2} \geq \frac{d_{B\bar{R}}\mathcal{J}_\mu(\delta)}{(1 - \sqrt{\mathcal{J}_\mu(\delta)})^2} \right\} \\ &= \mathbb{P}\left\{ \frac{d_{B\bar{R}}^2 \sum_{i \neq j} (\Upsilon_{B\bar{R}})_{ij}^2}{(1 - \mu)^2} \geq \frac{d_{B\bar{R}}\mathcal{J}_\mu(\delta)}{(1 - \sqrt{\mathcal{J}_\mu(\delta)})^2} \right\} \\ &\leq \mathbb{P}\left\{ \frac{\|\Upsilon_{B\bar{R}} - \frac{\mathbb{1}}{d_{B\bar{R}}}\|_2^2}{(1 - \mu)^2} \geq \frac{\mathcal{J}_\mu(\delta)/d_{B\bar{R}}}{(1 - \sqrt{\mathcal{J}_\mu(\delta)})^2} \right\} \quad (\text{D14}) \\ &= \mathbb{P}\left\{ \left\| \Upsilon_{B\bar{R}} - \frac{\mathbb{1}}{d_{B\bar{R}}} \right\|_2^2 \sum_{\ell=0}^{\infty} (1 + \ell) \mu^\ell \geq \frac{\mathcal{J}_\mu(\delta)/d_{B\bar{R}}}{(1 - \sqrt{\mathcal{J}_\mu(\delta)})^2} \right\} \\ &\leq \mathbb{P}\left\{ \sum_{\ell=0}^{\infty} (1 + \ell) (d_{B\bar{R}})^{\ell/2} \left\| \Upsilon_{B\bar{R}} - \frac{\mathbb{1}}{d_{B\bar{R}}} \right\|_2^{\ell+2} \geq \frac{\mathcal{J}_\mu(\delta)/d_{B\bar{R}}}{(1 - \sqrt{\mathcal{J}_\mu(\delta)})^2} \right\}, \end{aligned}$$

where we have wrote the Taylor series for  $1/(1 - \mu)^2$ , which converges as  $0 \leq \mu < 1$ , and finally used Eq. (D12). We have also used Eq. (D13) in the fifth and final lines. From here, we need to be careful in handling the probabilities. We will use that  $\mathbb{P}\{a(t) + b(t) > A + B\} \leq \mathbb{P}\{(a(t) > A) \cup (b(t) > B)\}$ . Then, also expanding the lower bound within

the probability brackets as a Taylor series,

$$\begin{aligned}
\mathbb{P}\left\{\tilde{\zeta}(\Upsilon, \mathcal{K}_b) \geq \frac{\mathcal{J}_\mu(\delta)}{(d_{B\bar{R}} - 1)(1 - \sqrt{\mathcal{J}_\mu(\delta)})^2}\right\} &= \mathbb{P}\left\{\sum_{\ell=0}^{\infty} (1 + \ell)(d_{B\bar{R}})^{\ell/2} \left\|\Upsilon_{B\bar{R}} - \frac{\mathbf{1}}{d_{B\bar{R}}}\right\|_2^{\ell+2} \geq \sum_{\ell=0}^{\infty} (1 + \ell)(d_{B\bar{R}})^{\ell/2} \left(\frac{\mathcal{J}_\mu(\delta)}{d_{B\bar{R}}}\right)^{(\ell+2)/2}\right\} \\
&\leq \mathbb{P}\left\{\bigcup_{\ell} \left((1 + \ell)(d_{B\bar{R}})^{\ell/2} \left\|\Upsilon_{B\bar{R}} - \frac{\mathbf{1}}{d_{B\bar{R}}}\right\|_2^{\ell+2} \geq (1 + \ell)(d_{B\bar{R}})^{\ell/2} \left(\frac{\mathcal{J}_\mu(\delta)}{d_{B\bar{R}}}\right)^{(\ell+2)/2}\right)\right\} \\
&= \mathbb{P}\left\{\bigcup_{\ell} \left(\left\|\Upsilon_{B\bar{R}} - \frac{\mathbf{1}}{d_{B\bar{R}}}\right\|_2^2 \geq \frac{\mathcal{J}_\mu(\delta)}{d_{B\bar{R}}}\right)\right\} \tag{D15} \\
&= \mathbb{P}\left\{\left\|\Upsilon_{B\bar{R}} - \frac{\mathbf{1}}{d_{B\bar{R}}}\right\|_2^2 \geq \frac{\mathcal{J}_\mu(\delta)}{d_{B\bar{R}}}\right\} \leq \mathcal{G}_\mu(\delta)
\end{aligned}$$

Where we have used that  $(a^\ell \leq b^\ell) \iff (a^k \leq b^k)$  for positive  $a$  and  $b$ , and non-negative integers  $\ell$  and  $k$ . In the final line applied the concentration of measure result Eq. (D1).  $\square$

---